

# Effects of quenching protocols based on parametric oscillators

Mariagiovanna Gianfreda<sup>a</sup>, Giulio Landolfi<sup>b,2</sup>

Department of Physics, Washington University, St. Louis, MO 63130, USA

Dipartimento di Matematica e Fisica "Ennio De Giorgi", Università del Salento and INFN Sezione di Lecce, 73100 Lecce, Italy

## ARTICLE INFO

### Keywords:

Parametric oscillator  
Ermakov equation  
Time-dependent Schrödinger equation  
Lewis-Riesenfeld invariant method  
Squeezing  
Quantum correlations

## ABSTRACT

We consider the problem of understanding the basic features displayed by quantum systems described by parametric oscillators whose time-dependent frequency parameter  $\omega(t)$  varies continuously during evolution so to realise quenching protocols of different types. To this scope we focus on the case where  $\omega(t)^2$  behaves like a Morse potential, up to possible sign reversion and translations in the  $(t, \omega^2)$  plane. We derive closed form solution for the time-dependent amplitude of quasi-normal modes, which is the very fundamental dynamical object entering the description of both classical and quantum parametric oscillators, and highlight its significant characteristics for distinctive cases arising based on the driving specifics. After doing so, we provide an insight on the way quantum states evolve by paying attention on the position-momentum Heisenberg uncertainty principle and the statistical aspects implied by second-order correlation functions over number-type states.

## 1. Introduction

Time-dependent quadratic hamiltonians play a fundamental role in physics and have been therefore intensively studied both at the classical and the quantum level. As a matter of fact, they have widespread applications including quantum optics and quantum information [1, 2, 3, 4, 5, 6, 7, 8], quantum cosmology [9, 10, 11, 12, 13, 14], plasma physics [15, 16, 17], disordered systems [18], and Bose-Einstein condensates [19, 20, 21, 22, 23, 24]. Phenomena thus appear in these areas of interest that share common features and similar originating mechanisms, e.g. the formation of wave patterns in spectra of dynamical variables and the creation of modes during the evolution of quantum fields. These aspects are currently inspiring experiments and the interplay between researchers involved in different areas. Indeed, the impressive progresses we are witnessing on the technological side open up to the possibility to probe time-dependent quadratic hamiltonian models subjected to variant parametric drivings and make more feasible the test of fundamentals of a theory, either directly or comparatively [17, 25, 26, 27, 28]. Interesting examples are provided by the electron-hole plasma created on the surface of a semiconductor slab by means of laser pulses, an experimental setup that has been discussed as a mirror for the nonstationary Casimir effect inside a cavity with moving boundaries [17, 25], and by atomic superfluids whose interaction strength is modified by Feshbach tuning, such as in [26] where authors laser cooled and Bose condensed cesium atoms in an optical dipole trap and then generated a quench of the atomic interaction resembling the change of gravitational field after inflation.

The recent very much improved capability to control materials properties, and the consecutive growing general interest in implementing *active* devices through time-varying media [2, 4, 29, 30] for applications of various kind, motivate a systematized collection of cases study providing intelligible and accurate predictions in respect to the evaluation of the dynamical responses of parametric oscillator systems; see also the discussion within the Bose-Einstein condensation context [23]. This would enable also one to gain a better knowledge of which conditions (initial state, control parameters) may turn out more advantageous for each definite application (see e.g. discussions in the context of superconducting circuit technology [28, 31, 32]) for which a quenching protocol is designed through parametric oscillators or related hamiltonian models as those in [33].

In this paper we fix some specific time dependent frequencies  $\omega(t)$  and address the study of one-degree of freedom quantum systems described by a parametric oscillator hamiltonian operator. We are aimed at giving an account on the way on the oscillation mechanism that arise at the classical level for the amplitudes of non-stationary modes is influenced by deviation from adiabaticity, how it is inherited at the quantum level, and the influence it has on quantum

\*Corresponding author: G. Landolfi

ORCID(s): 0000-0002-7352-2673 (M. Gianfreda); 0000-0001-6699-7876 (G. Landolfi)

<sup>1</sup>Maria.Gianfreda@le.infn.it

<sup>2</sup>giulio.landolfi@unisalento.it, giulio.landolfi@le.infn.it

correlations. Having this in mind, we shall perform therefore a study concerned with another solvable example of a time-dependent quadratic problem: a square parametric frequency functions  $\omega^2$  assuming a form connected with that of Morse potential function. Acting on a Morse potential shape through possible time-translations and sign-reversions will enable us to analyze, within a single analytical problem, the role played by changes in the energy subtraction/pumping scheme, such as whenever parameter are chosen in a way that asymmetrical barrier or well show up and a monotonicity is lost for  $\omega(t)^2$ , or giving rise to changes that perform non-adiabatically on a finite time-scale. We discuss extensively features of solution to the classical equation of motion, specifically their amplitudes  $\sigma$ . The step put in the position to build a solid bridge leading to the quantum dynamics. While dealing with time-dependent quadratic Hamiltonian systems and their dynamical comportments, a convenient guideline is the known fact that their quantum dynamics is in actuality ruled by the classical one: expectation values follow the classical motion *exactly*, and the spreading of solutions to Schrödinger can be understood in classical terms; see e.g. [34, 35, 36, 37, 38]. For this reason one should be well acquainted with features of the classical dynamics, and particularly of amplitudes  $\sigma$  of solution to the classical equation of motion. Indeed, it is the amplitude function  $\sigma$  that is later recognized to play the pivotal role in the quantum description of parametric oscillator dynamics. Functions  $\sigma$  obey by the Ermakov differential equation

$$\ddot{\sigma}(t) = -\omega(t)^2 \sigma(t) + \frac{c}{\sigma(t)^3}, \quad (1)$$

where dots denote time derivatives,  $\omega(t)$  is the time-dependent driving frequency, and  $c$  is a real positive constant parameter (merely acting as a scale factor for  $\sigma$ ). Solutions to Equation (1), and their time-differential  $\dot{\sigma}$ , specialize the classical system orbits in phase-space, and in turns this determines the elements of the position-momentum correlation matrix among quantum wave-packets solving the Schrödinger equation [36, 37]. This is an instance of what is arguably the most profound connection of quantum mechanics with the classical one: the uncertainty principle, in its Robertson-Schrödinger strong form, relies on the existence of Poincaré invariants on the classical side [39, 40, 37, 41, 42], the Planck's constant simply representing a scale requirement. For the one degree of freedom systems ruled by the time-dependent parametric oscillator hamiltonian, the basic invariant is the area the ellipses in phase space determined for assigned values of the so-called Ermakov invariant, a quadratic Nöther invariant for the system [43]. Their deformation in the course of dynamics is ruled by the amplitude  $\sigma$  changes, whose oscillatory features intertwine with those of classical Newton equation of motion for the parametric oscillator, a Sturm-Liouville problem indeed. Oscillations for classical orbits consequently drive the squeezing on cognate Wigner ellipses at the quantum level. Peculiar oscillating phenomena therefore enter quantum correlation functions and mode-counting statistics. Examples will be given of highly oscillating amplitudes determining strong squeezing phenomena in phase-space, and of the manner they steer the mode-counting statistics.

The outline of the paper is as follows. In Section 2, we provide a recap of the treatment of time-dependent quadratic quantum systems through the Lewis-Riesenfeld invariant approach [44]. After recalling the linkage between the parametric oscillator and the Ermakov equations, in Section 3 we make some general comments on the features of their solutions. In Section 4, we present figures showing solution to Ermakov equation based on suitable initial conditions and representative sets of parameters entering the time-frequency function  $\omega(t)$  we opted for, and analyze thoroughly the features displayed. In Section 5 we pay attention on implied squeezing of classical Ermakov ellipses in phase-space, which really means to comprehend the Heisenberg uncertainties for position-momentum operators at the quantum level. In Sections 6 and 7 our attention is devoted to mode-counting statistics. There, we consider normalized second order correlation functions pertinent nonclassical states of the number type and argue on the typicalities that are visible from their plots. Section 8 will be for conclusions. Finally, in Appendix A, we expound the derivation of the solutions to the parametric oscillator equation for the frequency parameter we have chosen and determine their Wronskian, a task needed to the construction of analytical solutions to Ermakov equation (1).

## 2. Quantum parametric oscillator: a brief on the theoretical background

The quantization of time-dependent quadratic systems is a well established topic, see e.g. [37, 36]. The most effective way to proceed has been recognised in the approach proposed by Lewis and Riesenfeld in [44], a method intrinsically relying on the identification of symmetries and invariants. In this Section we recall the basic steps connecting the solutions to the Schrödinger equation pertinent to a parametric oscillator hamiltonian operator to the spectral problem for the quantum Ermakov invariant operator. After doing so, the Bogolubov map relating the invariant description to Schrödinger picture is presented. This will enable us to delineate the squeezing dynamics experienced by the system.

## 2.1. The Lewis-Riesenfeld approach to quantum parametric oscillator

Consider the time-dependent one-dimensional Hamiltonian

$$H(t) = \frac{p^2}{2m} + \frac{m\omega^2(t)}{2}q^2, \quad (2)$$

where  $q$  and  $p$  are operators that satisfy the canonical commutation relation  $[q, p] = i\hbar$ . The mass parameter  $m$  is not time dependent. For systems governed by the hamiltonian operator (2), a convenient description can be given in terms of a time dependent hermitian operator  $I \equiv I(t)$  which is an invariant; that is,  $I^\dagger = I$  and  $\dot{I} = \partial_t I + (i\hbar)^{-1} [I, H] = 0$ , where the dot stands for the total time derivative. A state vector  $|\psi(t)\rangle$  that satisfies the Schrodinger equation for (2),  $i\hbar \partial_t |\psi(t)\rangle = H(t)|\psi(t)\rangle$ , can be written in terms of the time-dependent eigenstates  $|\phi_n(t)\rangle$  associated to the invariant  $I(t)$  with time-independent eigenvalues  $\lambda_n^{(I)}$ ,  $I |\phi_n(t)\rangle = \lambda_n^{(I)} |\phi_n(t)\rangle$ , via the general superposition formula  $|\psi(t)\rangle = \sum_{n=0}^{\infty} c_n e^{i\alpha_n(t)} |\phi_n(t)\rangle$ , where the phase  $\alpha_n(t)$  satisfies the equation

$$\hbar \dot{\alpha}_n = \langle \phi_n | i\hbar \partial_t - H | \phi_n \rangle. \quad (3)$$

By assuming that  $I(t)$  can be written as a quadratic expression in the dynamical variables  $q$  and  $p$ , one can find that

$$I = \frac{c}{\sigma^2(t)} q^2 + \left[ \sigma(t) \frac{p}{m} - \dot{\sigma}(t) q \right]^2, \quad (4)$$

where  $\sigma(t)$  is a real function of time, solution to the Ermakov differential equation (1). Operator (4) is essentially the quantised version of the classical invariant discussed originally by Ermakov in his prime analysis in [57]. The invariant operator  $I(t)$  in Equation (4) can be written as

$$I(t) = \frac{2\sqrt{c}\hbar}{m} \left[ a^\dagger(t) a(t) + \frac{1}{2} \right], \quad a(t) = \frac{1}{\sqrt{2\hbar}} \left[ \frac{c^{1/4}\sqrt{m}}{\sigma} q + i \left( \frac{\sigma}{\sqrt{m}c^{1/4}} p - \frac{\sqrt{m}\dot{\sigma}}{c^{1/4}} q \right) \right]. \quad (5)$$

Operators  $a(t)$  and  $a^\dagger(t)$  are time-dependent operators of the annihilation and creation type, satisfying the canonical commutation rule  $[a(t), a^\dagger(t)] = 1$ . Accordingly,  $N = a^\dagger(t) a(t)$  is an operator of the number type, from which it follows that the spectrum of  $I(t)$  consists in the set of stationary eigenvalues  $\lambda_n^{(I)} = \sqrt{c} m \hbar (n + \frac{1}{2})$ , for  $n = 0, 1, 2, \dots$ , and the eigenstates are the same of the number operator  $N$ ,  $|\phi_n(t)\rangle \equiv |n\rangle$  being  $N|n\rangle = n|n\rangle$ . Otherwise said, the invariant operator  $I(t)$  can be mapped into a time-independent harmonic oscillator via a unitary transformation (see e.g. [45]). This implicitly states that Fock-type spaces are defined at different times in terms of the common eigenstates  $|n\rangle$  of the number operator  $N$  and Ermakov invariant  $I$ , and that these spaces can be then mapped one into the other through a time-dependent transformation. Similarly, coherent-like bases at different times may be defined by means of the eigenstates  $|\alpha\rangle$  associated with the spectral problem for the time-dependent operator  $\hat{a}$ , i.e.  $\hat{a}|\alpha\rangle = \alpha|\alpha\rangle$ . These are the so-called Lewis-Riesenfeld coherent states (thought they are actually squeezed states), and are expressible in terms of the states  $|n\rangle$  through the usual relationship. The number-type states  $|n\rangle$ , and consequently the coherent-type states  $a$  *l* Lewis-Riesenfeld  $|\alpha\rangle$ , do not solve the Schrodinger equation for the Hamiltonian operator (2). For this to happen the action of a unitary operator is needed that merely equips each component  $|n\rangle$  with the proper time-dependent phase  $\alpha_n$  defined via (3), an operation that do not affect means over  $|n\rangle$  or  $|\alpha\rangle$  and let these states be of interest for practical purposes. As in the standard harmonic oscillator case, exact analytical solutions in the form of gaussian wave-packets can be therefore found for the Schrödinger equation associated to a parametric oscillator hamiltonian. A strong connection is consequently established between classical and quantum dynamics. In fact, the time-evolution of the maximum and the width of a wave-packet (the two quantities that uniquely determine it) are governed by classical dynamics: the maximum behaves like a particle following just the classical trajectory and the width is proportional to the amplitude  $\sigma$  of solution to classical Newton-Lagrange equation for the parametric oscillator [34, 36].

## 2.2. Unitary Bogolubov transformation for annihilation-creation operators

The identification of features associated with the dynamics for the quantum systems described by the hamiltonian (2) can be addressed by resorting to a squeezing formalism [46]. This can be done by writing

$$a(t) = \mu(t) a_0 + \nu(t) a_0^\dagger, \quad |\mu|^2 - |\nu|^2 = 1 \quad (6)$$

where  $a_0$  and its hermitian conjugate  $a_0^\dagger$  are the ladder-type operators applicable to the fixed-time hamiltonian operator at an initial instant  $t_0 = 0$ , i.e.

$$H_0 \equiv H(0) = \frac{p^2}{2m} + \frac{1}{2} m \omega_0^2 q^2 = \hbar \omega_0 \left( a_0^\dagger a_0 + \frac{1}{2} \right), \quad \omega_0 \equiv \omega(0), \quad (7)$$

$$a_0 = \sqrt{\frac{m \omega_0}{2\hbar}} q + \frac{i}{\sqrt{2\hbar m \omega_0}} p. \quad (8)$$

The constraint  $|\mu|^2 - |\nu|^2 = 1$  on Bogolubov coefficients  $\mu, \nu$  follows from the unitarity of transformation. We have:

$$\mu(t) = \frac{1}{2 c^{1/4} \sqrt{\omega_0}} \left( \frac{\sqrt{c}}{\sigma} + \omega_0 \sigma - i \dot{\sigma} \right), \quad \nu(t) = \frac{1}{2 c^{1/4} \sqrt{\omega_0}} \left( \frac{\sqrt{c}}{\sigma} - \omega_0 \sigma - i \dot{\sigma} \right) \quad (9)$$

(close formulae can be given when the mass-type parameter is time-dependent [47]; adaptation to SUSY-QM formalism can be found in [48]).

Any element  $|m\rangle$  of the Fock space determined by the invariant  $I(t)$  spectral problem at time  $t$ , i.e. a state  $|m\rangle$  obtained by application of  $(\hat{a}^\dagger)^m$  on the  $\hat{a}$ -vacuum  $|0\rangle$ , can be expressed as an infinite superposition of the number states  $|n\rangle_0$  belonging to the Fock space associated with the operators  $\hat{a}_0$  and  $\hat{a}_0^\dagger$ , for which  $\hat{N}_0 |n\rangle_0 = \hat{a}_0^\dagger \hat{a}_0 |n\rangle_0 = n |n\rangle_0$ . The fundamental overlaps  ${}_0\langle n|m\rangle$  are established via Eqs. (6) and (9), and so the evolution of arbitrary wave-functions can be obtained accordingly in either of the basis (for the explicit form of states  $|m\rangle$  in position representation, see e.g. [36, 37, 3]). Notice that at this stage there is a freedom in respect to the choice of initial condition for the Ermakov differential problem (1), and this also affect the explicit form of Bogolubov mapping. Unitarily inequivalent time-dependent vacua can be thus introduced via  $a(t)|0\rangle = 0$  by the general form of the invariant factorization, Eq (5). This is not surprising, as it generalizes to the non-autonomous case the well understood unitary action of squeezing of orbits for the stationary case. To remove the vacuum ambiguity, in this paper we shall proceed in the most economical way, i.e. by demanding that at initial time  $t = 0$  the operator  $a(0)$  coincides with  $a_0$  in (8):  $\mu(0) = 1$  and  $\nu(0) = 0$ . This requirement fixes initial conditions to the Ermakov equation (1) as follows:

$$\sigma_0 \equiv \sigma(0) = \frac{c^{1/4}}{\sqrt{\omega_0}}, \quad \dot{\sigma}_0 \equiv \dot{\sigma}(0) = 0. \quad (10)$$

Evidently, the Hamiltonian and the invariant operators do not generally commute,  $[I, H] = (\mu \nu^* \hat{a}_0^2 - h.c.)$ . But once initial conditions (10) are superimposed Lewis-Riesenfeld states at initial time coincide with standard states for the fixed-time harmonic oscillator with frequency  $\omega_0$ . Of course other choices can be made for  $\mu(0)$  and  $\nu(0)$  that more conveniently may allow to follow the evolution of other states.

### 3. Solutions to Ermakov equation: general aspects

Ermakov systems have widespread occurrence mathematics and physics [49, 50, 51, 52, 53, 54, 55, 56] as they naturally arise once, in the spirit of the pivotal Ermakov and Böhl discussions [57, 58], solutions to second order linear differential equations are expressed via the sine and the cosine functions [59]. In practice, the Ermakov equation (1) is nothing but one of the two differential constraints into which the classical parametric oscillator equation

$$\ddot{x}(t) + \omega^2(t) x(t) = 0 \quad (11)$$

splits once solutions are sought in the quasi-normal mode form

$$x = \frac{\sqrt{I_{cl}}}{\sqrt{c}} \sigma(t) \cos[\theta(t) + \bar{\theta}_0] \quad (12)$$

with real constants  $\bar{\theta}_0$  and  $I_{cl}$ ,  $c > 0$ , the other differential constraint to be satisfied for consistency determining the phase function via  $\dot{\theta} = \sqrt{c} \sigma^{-2}$ . The constant  $I_{cl}$  in (12) corresponds to the value assumed by the Noether invariant of the theory obtained by taking  $q$  and  $p$  in (4) as the classical position and momentum phase-space coordinate. Relying

on this connection between the two differential problems, it is possible to employ solutions to the linear parametric equation to the purpose of desuming solutions to the nonlinear Ermakov amplitude equation (1). In exact terms, the general solution to Eq. (1) can be expressed in terms of two linearly independent solutions  $x_1$  and  $x_2$  of (11) via

$$\sigma = \sqrt{A x_1^2 + 2 B x_1 x_2 + C x_2^2}, \quad (13)$$

with the condition

$$A C - B^2 = \frac{c}{W^2(x_1, x_2)} \geq 0, \quad (14)$$

where  $W$  is the Wronskian of  $x_1$  and  $x_2$ . The Ermakov-Böhl-type formulae (13)-(14) generalize those with  $B = 0$  considered at early stages [58, 57], and can also be derived brightly using projective geometry [50]. The constants  $A, B, C$  can be completely fixed by imposing (14) along with initial conditions on  $\sigma$  and  $\dot{\sigma}$ . Real solutions of Ermakov equation are thus positively defined and do not vanish.

The behavior of solutions to the Ermakov equation (1) is obviously a reflex of features that are typical of solutions to the parametric oscillator differential equation (11). The presence of oscillating patterns for  $\sigma$  can be awaited on the basis of the fundamental results obtained for equations of the parametric oscillator type [60, 61, 62]. The well-known Fite-Leighton criterion, for instance, states that if  $f(t)$  is a nonnegative real function in the interval  $t \in [t_0, \infty)$  such that  $\lim_{T \rightarrow \infty} \int_{t_0}^T f(t) dt = \infty$  then the equation  $\ddot{x}(t) + f(t)x(t) = 0$  is *oscillatory*, i.e. has arbitrarily large zeroes on the independent variable domain  $[t_0, \infty)$ . When  $f(t)$  is allowed to assume negative values for arbitrarily large values of  $t$ , the Wintner theorem can be applied, according to which if  $\lim_{T \rightarrow \infty} (1/T) \int_{t_0}^T dt \int_{t_0}^t f(t') dt' = \infty$  the equation is oscillatory. Furthermore, the Sturm comparison theorem supports the conclusion that the larger is the parametric frequency the more rapidly solutions to the parametric oscillator equation will oscillate, and the Sturm separation theorem guarantees that given two linear independent solutions of the parametric oscillator equation the zeros of the two solutions are alternating. These results provide a convenient platform for appraising implications for the solutions to the Ermakov equation owing to the connection established via (13)-(14). Independent solutions for the parametric oscillator equation that alternate zeros introduces indeed a mechanism where terms in (13) alternate minor and major contribution, and the function  $\sigma$  consequently displays undulations that can be sustained to different degrees depending the specific form of independent solutions (i.e. on the shape of  $\omega(t)$ ) and on coefficients  $A, B, C$  (i.e. on the initial conditions for the Ermakov equation; see also the discussion in [63] appertaining the constant frequency case). In respect it is worth to recall that the inequality

$$|x| \leq (|x(t_0)| + |\dot{x}(t_0)|) e^{\int_{t_0}^t |f(s)-1| ds}. \quad (15)$$

(in proper units) generally holds [62]. The polar form of Ermakov-Böhl decomposition (12) then allows to transfer the inequality (15) directly to an inequality for the amplitude  $\sigma$  comprising initial conditions for the Ermakov equation. Adiabaticity of variations for the frequency parameter  $\omega$  do not suffice to guarantee that even changes for  $\sigma$  are realised slowly. Attention has to be paid on the right-hand side of Equation (1). Demanding its vanishing functions as retaining the leading order in the WKBJ expansion treatment of the parametric equation [62, 64]. As long as  $\omega^2 \sigma^4$  deviates from attaining values about  $c$ , the dynamical changes in amplitude  $\sigma$  are less smooth. Accordingly, phases  $\theta$  deviate from the nearly linear behavior of the adiabatic regime (bear in mind that  $\theta$  directly determines the quantum phases resulting from (3) over number-type states through to the relation  $\dot{\alpha}_n(t) = -(n + 1/2)\sqrt{c} \sigma^{-2}$  [44], i.e.  $\dot{\alpha}_n(t) = -(n + 1/2)\dot{\theta}(t)$ ).

#### 4. Analysis of amplitudes $\sigma$ for oscillators with Morse-type square frequencies

In this communication we consider a time-dependent quadratic system (2) with square parametric frequency

$$\omega^2(t) = D_e \left[ e^{-\frac{2(t+t_g)}{b}} - 2 e^{-\frac{t+t_g}{b}} \right] + V_\infty, \quad (16)$$

where  $D_e \neq 0$ ,  $b > 0$  and  $V_\infty \neq 0$  are real parameters. The form of Equation (16) basically represents a generalization in the time-domain of the well-known Morse potential, which is indeed recovered for  $V_\infty = 0$ , where the parameters  $D_e$  and  $b$ , both positive, determine the depth and the effective width of the Morse potential hole, see Figure 1. Adopting

(16) we also consider a possible upside-down flipping caused by the change of sign of  $D_e$ , as well as horizontal translation of the standard Morse curves via  $t \rightarrow t + t_s$ . This enables us to design different types of drivings, and to argue on the problem with a wider generality. To this, it is convenient (especially for the analytical treatment, Appendix A) to distinguish four cases relying on the signs of parameters  $D_e$  and  $V_\infty$ : i) Case 1,  $D_e, V_\infty < 0$ ; ii) Case 2,  $D_e < 0, V_\infty > 0$ ; iii) Case 3,  $D_e, V_\infty > 0$ ; iv) Case 4,  $D_e > 0, V_\infty < 0$ . As we will see, further restrictions on parameters can arise because we shall be obviously concerned only with the cases for which  $\omega(t) \geq 0$ , and it shall be understood that

$$\omega_0 \equiv \omega(0) = \sqrt{D_e(e^{-2t_s/b} - 2e^{-t_s/b}) + V_\infty} \quad (17)$$

is strictly positive. The qualitative behavior for the  $\omega^2$ 's we shall deal with separately in each case is outlined in Figure 1.b).<sup>1</sup>

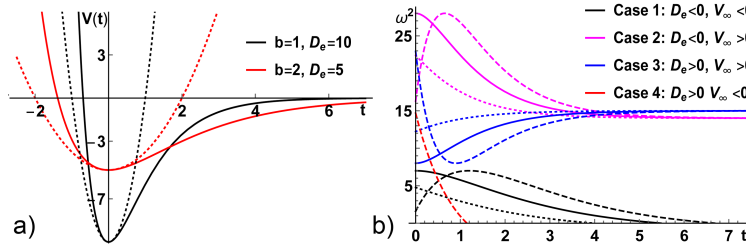


**Figure 1:** a) Morse potential  $V(t) = D_e(e^{-\frac{2t}{b}} - 2e^{-\frac{t}{b}})$  compared to its harmonic approximation (dotted). b) Examples of admissible  $\omega^2(t)$  once all the possible actions on the Morse potential (sign reversion, vertical and horizontal shifts) are put forward via Eq. (16); solid, dashed and dotted curves refer to null, negative and positive time-translation parameters  $t_s$ .

When  $V_\infty < 0$  the dynamical study can be carried out thoroughly for all times  $t \geq 0$  (Cases 2 and 3), otherwise a positive time-dependent square frequency rules the dynamics only over a finite time window (Cases 1 and 4) whose duration is determined through the root of equation  $\omega^2 = 0$  defined via

$$t_+ = -t_s - b \log \frac{D_e + \sqrt{D_e(D_e - V_\infty)}}{D_e}. \quad (18)$$

In this Section, we analyse solutions  $\sigma$  to Ermakov equation (1) when  $\omega^2$  takes the Morse-like form (16) and the parameters involved are varied to modify width and height of barriers/holes as well as the position of the curve in the  $(t, \omega^2)$  plane. Attention will be also paid on phases  $\theta = \sqrt{c} \int_0^t \sigma^{-2} dt$ . The examination can be conducted being conscious that the Fite-Leighton criterion applies in a natural manner to Cases 2 and 3, for which  $V_\infty, b > 0$ , and it is legitimate to consider the asymptotic limit  $t \rightarrow \infty$ , that yields indeed to  $\lim_{T \rightarrow \infty} \int_{t_0}^T \omega^2(t') dt' = \infty$ . In Cases 1 and 4, application of Wintner theorem interdicts the independent solutions to the equation  $\ddot{x} + \omega^2 x = 0$  from possessing arbitrarily large zeroes. Nevertheless, in our study this differential problem is actually posed in a finite interval for the time independent variable. Zeroes in this interval are not excluded and, depending on the manner initial conditions and parameters are fixed, visible fluctuations may be produced. Also notice that the outcome of integration in (15) (with parametric frequency cast in adimensional units) is always finite, even as  $t \rightarrow \infty$  (in Cases 2 and 3 where the limit makes sense). Hence solutions to parametric and Ermakov equations are bounded, but initial conditions may determine high upper bounds even when small variations of  $\omega$  take place.

Features of the solutions to Ermakov equation in each of the four cases will be argued in the following Subsections with plots summarising their behavior for different values of the parameters involved and the initial conditions (10). The implication at the classical level of such "instantaneous no-squeezing" condition is that it shapes parametric oscillator solutions (12) that at the initial time reproduce what one gets at the same time for the standard representation of stationary modes for harmonic oscillators with mass  $m$ , proper frequency  $\omega_0 \equiv \omega(0)$ , constant amplitude and phase

<sup>1</sup>Actually, curves like the red one in Fig. 1.b) can be obtained also in Case 1 for extremely large negative  $D_e$ . However, for the sake of an advantageous schematic that makes a more net contradistinction between drivings with different features, we shall exclude these kind of choices for Case 1 and shall designate Case 4 for the analysis of dynamics under strongly non-adiabatic decreasing drivings ceasing in finite time.



depending linearly on time. In different words, the curve determined in phase-space by the Ermakov invariant at  $t = 0$  is just a rescaling by a factor  $2\sqrt{c}/m\omega_0$  of the elliptic orbit of the harmonic oscillator with frequency  $\omega_0$  and mass  $m$ , of which it preserves the minor/major axes ratio.

The following forewarnings are in order. Firstly, to avoid that the more mathematical details break the overall flow and affect the readability of the paper, the derivation of the formulae that are necessary to construct closed form solutions to the Ermakov equation (1) via Eqs. (13)-(14) will be worked out separately in Appendix A.<sup>2</sup> There the independent solutions to Equation (11) are shown to be given in terms of the Tricomi confluent hypergeometric function  $U$  and the Kummer function of the first kind  ${}_1F_1$ , whose Wronskians are next computed. Secondly, being beneficial to the physical interpretation of results, hereinafter a reference to the frequency  $\omega(t)$  will often be present in plots through of dotted curves of the color of the principal quantities that will be evaluated with the same assignment of parameters; the way the reference to  $\omega(t)$  will be given is established case by case depending on individual plot's convenience. Finally, from now on all parameters entering the definition of the parametric frequency will be considered in adimensional units and it will be set  $c = 1/4$ .

#### 4.1. Case 1: $D_e, V_\infty < 0$

The first case that we consider is a square parametric frequency defined through an inverse Morse potential with a negative nonvanishing asymptotic value. It is realized with negative parameters  $D_e$  and  $V_\infty$ , and such that curve (16) intercepts the positive time axis once. The full set of parameters involved in (16) has also to guarantee that  $\omega_0^2 > 0$  (i.e. a correctly defined cognate harmonic oscillator at the initial time). Thence the two roots of  $\omega^2 = 0$  have to be real, noncoincident and opposite in sign. That means  $D_e < V_\infty < 0$  and  $-b \log(1 + \sqrt{1 - V_\infty/D_e}) < t_s < -b \log(1 - \sqrt{1 - V_\infty/D_e})$ .

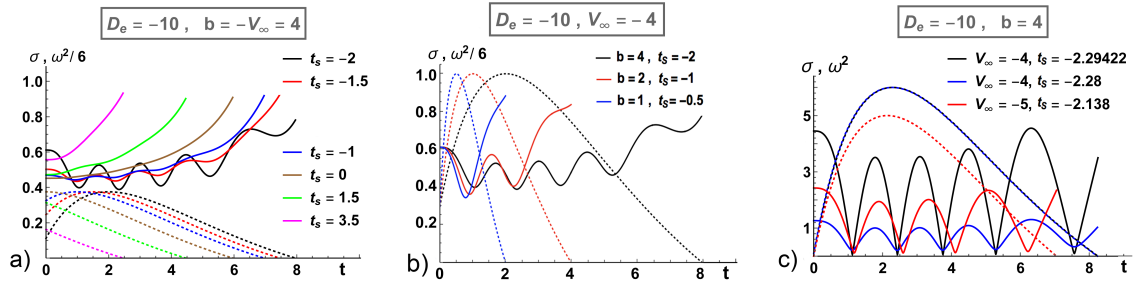


**Figure 2:** Function  $\sigma$  when  $\omega(t) > 0$  is defined via Eq. (16) with  $D_e, V_\infty > 0$ . Dotted curves refer to scaled  $\omega^2$ . a) Examples for fixed  $D_e, V_\infty, b$  and varying  $t_s$ . b)  $t_s < 0$ . Generation of an oscillating pattern shown by considering three different drivings with the same initial and maximum values, but progressing with different rates and over distinct time windows. c)  $t_s < 0$ . Turning on at the initial time faster varying parametric drivings gives rise to greater fluctuations.

Curves in Figure 2 summarize the typical behavior for  $\sigma$  in this case upon superimposition of the initial conditions (10). For  $t_s = 0$ , solutions to the Ermakov equation tend to increase their value during the course of evolution in a way similar to the brown curve in Fig. 2.a). When  $t_s \neq 0$  the resulting horizontal translations of the parametric frequency shape deform solutions  $\sigma$  in ways that may lead to significantly different curves even if the changes in the shift parameter  $t_s$  appear commensurable. Besides the obvious remark in respect to the quantitative change in the initial value of  $\sigma$ , from the analytical point of view it is to point out that evolution now would no longer start at an instant when the time-differential of the frequency parameter vanishes. This circumstance plays a role in the manner the system dynamics deviates from comportment it would display if  $t_s = 0$ . With the increasing of  $t_s > 0$  the time interval where dynamics occur diminishes while the initial value  $\sigma_0$  increases, and the initial slowly varying portion of  $\sigma$  shrinks, Fig. 2.a). Moving to the case  $t_s < 0$ , the curve  $\omega(t)$  grows until it reaches its maximum value at  $t = -t_s$  to later decrease until its vanishing at  $t_+$ , Eq. (18). If the time interval  $[0, -t_s]$  is sufficiently wide, the initial value of  $\omega$  cuts down meaningfully. As Figures 2.a) and 2.c) show, the effect is quite a gain for the initial value for function  $\sigma$  and for the magnitude of

<sup>2</sup>Assuming the initial conditions (10), for the constants in Equation (13) one has:  $\omega_0 W(x_1, x_2)^2 A = \sqrt{c} [\omega_0^2 x_2^2(0) + \dot{x}_2(0)^2]$ ,  $\omega_0 W(x_1, x_2)^2 B = \sqrt{c} [\omega_0^2 x_1(0) x_2(0) + \dot{x}_1(0) \dot{x}_2(0)]$ , and  $\omega_0 W(x_1, x_2)^2 C = \sqrt{c} [\omega_0^2 x_2^2(0) + \dot{x}_2(0)^2]$ .

fluctuations occurring thereafter. Remark that in the plot 2.c) the  $\omega$ 's at initial time are very small, but never vanishing: resulting initial conditions for the corresponding  $\sigma$  are relatively large, but in fact finite. The point is that when  $t_s < 0$  a sign change occurs for  $\dot{\omega}$ . The system is thus required to adapt itself first to a continuous positive frequency jump  $\Delta_{\omega,1} = \omega_{max} - \omega_0 = |D_e - V_\infty| - \omega_0$ , and later to a continuous negative jump  $\Delta_{\omega,2} = \omega_{max} = |D_e - V_\infty|$ . Such a driving dynamics calls for a bigger adaptation effort as long as  $t_s$  takes more negative values, and this happening is communicated through enhanced oscillations for  $\sigma$ . Also note that when  $t_s < 0$  the mean value of  $\sigma$  tends to increase its value during the course of evolution after a transient time where it decreases. Such dynamics is related to the occurrence of a sign change for  $\dot{\omega}$ . Indeed, there is a basic general process by which variations of amplitude  $\sigma$

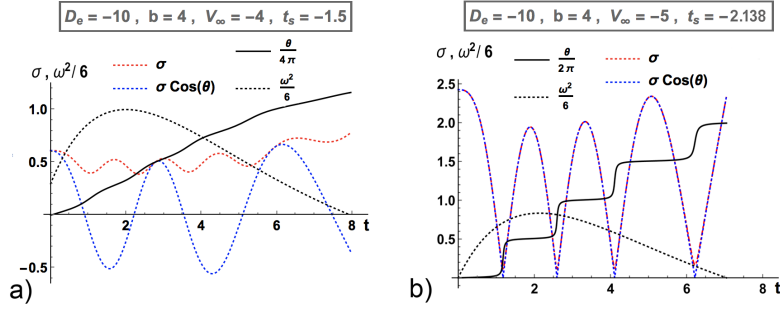


**Figure 3:** Comparison between solutions to the Ermakov equation  $\sigma$  and solutions to the parametric oscillator equation. When its oscillations increase due to non-adiabaticity of frequency changes and of dynamics, amplitude  $\sigma$  progressively acquires features of solutions to the parametric oscillator equation, approaching the positive portions of  $x = \sigma \cos \theta$  and the reflections across the time axes of negative ones. Accordingly, phases  $\theta$  develop continuous jumps.

are brought about: the raising of frequency parameter  $\omega$  acts to reduce  $\sigma$  and vice versa. If the frequency parameter varies adiabatically the correspondence is stronger: the lowest order term produced by application of WKBJ expansion method entails just a 1-to-1 map between parametric frequency  $\omega$  and quasi normal-mode amplitude  $\sigma$ , the relationship  $\dot{\theta} = \sqrt{c}/\sigma^2$  between amplitude and phase of quasi-normal modes effectively turning into  $\dot{\theta} \simeq \omega$ . By plotting  $\omega^2 \sigma^4 / c$  when  $t_s \geq 0$  is either vanishing or relatively small, one would see this function close to unity for most of the evolution before rapidly collapsing to zero when the driving  $\omega$  is going to be absolutely switched off; for higher values of the time-translation parameter  $t_s$ , the function  $\sigma$  would clearly reach the fast growth regime in a shorter time. With the decreasing of  $t_s < 0$ , prior the final vanishing of  $\omega^2 \sigma^4 / c$  one would instead view the onset and the escalating of net oscillations, with meaningful deviations from the adiabatic condition. That being the case, non-negligible fluctuations start to be generated for  $\sigma$ , with the progressive drawing near of solutions to the Ermakov equations and the absolute value of solutions  $\sigma \cos \theta$  to the parametric oscillator equation with the same initial conditions and frequency; see Figure (3). A staircase type shape ensues for the phase  $\theta$  with raisers developing in correspondence of minima for  $\sigma$ . Owing to the development of continuous phase jumps of the order of  $\pi$ , the function  $\cos \theta$  modifies to a sequence of square-wave like elements with minimum and maximum about the values -1 and 1.

Before to conclude the Subsection, we finally call attention on the fact that for the plots we have chosen frequency parameters so to exclude very strong variations for drivings. The relatively large time-scale parameter  $b$  we used allows to better visualise the small-to-large generation of fluctuations for the amplitude  $\sigma$ . Lowering  $b$ , the driving changes become faster, e.g. making a more peaked shape for  $\omega(t)$  about the maximum when  $t_s < 0$ . Wider fluctuations can be then expected. Since also the time interval where the parametric driving acts becomes smaller, only a part of the previously evidenced fluctuating patterns for  $\sigma$  may be realised, as shown in figure 3.c).

#### 4.2. Case 2: $D_e < 0$ and $V_\infty > 0$

The case we dwell upon in this Subsection differs from the previous one in that the parametric frequency tends to an asymptotic value  $V_\infty > 0$ , allowing for a potentially infinite time evolution. After a possible pulse-like driving, the system reaches exponentially fast a dynamical regime that basically act as an harmonic oscillator that is perturbed extremely weakly by a time-dependent correction to the frequency.

Let us analyze the solutions to the Ermakov equation in the present case once we set  $t_s = 0$  and the initial conditions (10). The frequency decreases monotonically from the initial value  $\sqrt{V_\infty + |D_e|}$ . Solution  $\sigma$  initially grows until it



stabilizes to an oscillating regime. For fixed height of the frequency parameter shape (i.e. for fixed  $D_e$ ), the magnitude of oscillation is strongly affected by the width of the time interval where  $\dot{\omega}$  is significant and the jump for  $\omega$  from maximum to asymptotic value is essentially realized. As long as the positive time-scaling parameter  $b$  increases, the amplitude of oscillations becomes smaller and smaller, the fluctuation being basically negligible for sufficiently large values of  $b$ . Magnitude of oscillations varies significantly provided that the different  $b$  are taken so to exclude at a too sudden initial jump for  $\omega$ . This is evident from Figure 4.a) (there the  $b = 0.1$  and  $b = 0.015$  curves almost overlaps). At the initial stage  $\sigma$  grows monotonically with very little visible fluctuations in the growth rate, as evidenced in Figure 4.b) where  $\dot{\sigma}$  is plotted for the smoothest curves in Figure 4.a). At fixed  $b$  and  $D_e$ , the greater is the asymptotic value of frequency parameter  $|V_\infty| > 0$  the lower are the values about which oscillations of  $\sigma$  are realized, as well as their amplitude and their characteristic period; see the comparison between the black curve and the (essentially overlapping) yellow and magenta ones in figure 4.a) as well as the blue curve in figure 4.c). For assigned  $V_\infty$  and  $b$ , the progressive augment of  $|D_e|$  results into more and more substantial departures of  $\omega^2$  from the "optimal" constant value  $V_\infty$ , and wider oscillation regimes arise with mean values of  $\sigma$  attaining higher values with respect to the stationary amplitude  $\sigma_{HO} = (c/V_\infty)^{1/4}$  of harmonic oscillators whose frequency is the asymptotic value  $\omega_\infty = \sqrt{V_\infty}$  of  $\omega(t)$ ; see Fig. 4.c).

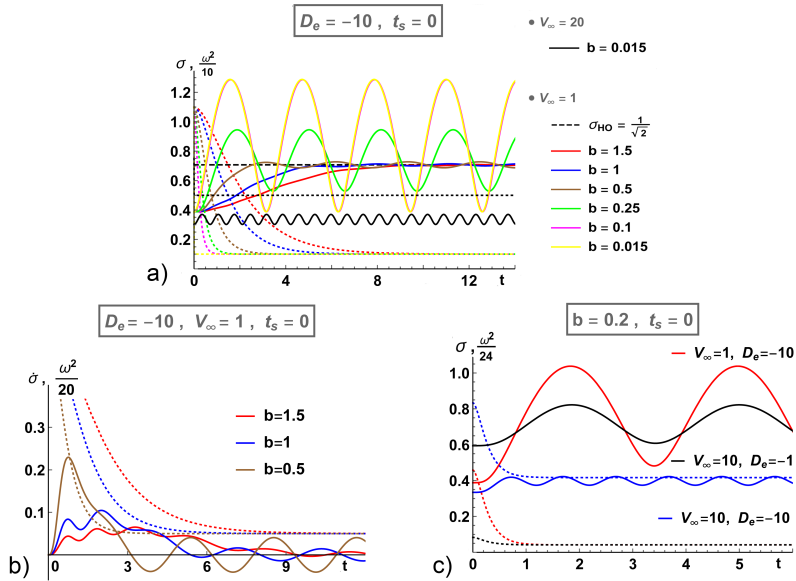


**Figure 4:** Function  $\sigma$  and  $\dot{\sigma}$  when  $V_\infty > 0$ ,  $D_e > 0$ ,  $t_s = 0$  in (16). Initial conditions are (10) with  $c = 1/4$ . Color dotted curves refer to corresponding potentials up to scaling factors. Oscillations of different magnitude are generated for  $\sigma$  depending on the properties of the acting parametric driving. In panel a) the reference value  $\sigma_{HO} = (c/V_\infty)^{1/4}$  is also shown for  $V_\infty = 1$ .

We can now proceed by considering a nonvanishing time-translation parameter  $t_s > -b \log(1 + \sqrt{1 - V_\infty/D_e})$ . By considering negative  $t_s$  and the initial conditions (10), the driving frequency turns from monotonic to unimodal in a manner that is, evidently, similar to the Case 1 argued in previous Subsection. By progressively diminishing the parameter  $t_s < 0$ , the newly introduced initial increasing behavior for  $\omega^2$  enters more and more effectively into action in a way that is in agreement with findings from Subsection A.1 and expectations from the WKBJ/adiabatic arguments. From Figures 5 one infers indeed that larger fluctuations are generated for lower negative values of  $t_s$ . Explicit examples are also provided concerning the repercussion of diversifying the time-scaling parameter  $b$ , as in plots 5.a) and 5.b) that make definite the resulting amplification of  $\sigma$ -oscillations (compare with Figs. 4.a) and 4.b)). Once again, it is found that mere adiabaticity of frequency changes is not enough to ensure a smooth outcome for  $\sigma$ . In contrast, if very gentle modifications of parametric frequency begin to rule the dynamics at a certain time, then oscillations of large magnitude keeps being sustained. This simply reflects the fact that the systems enters into that dynamical regime with a largely oscillating amplitude  $\sigma$  owing the features of the initial transient regime, and the very adiabatic changes of hamiltonian taking place thereafter are so extremely slow that they are not much effective

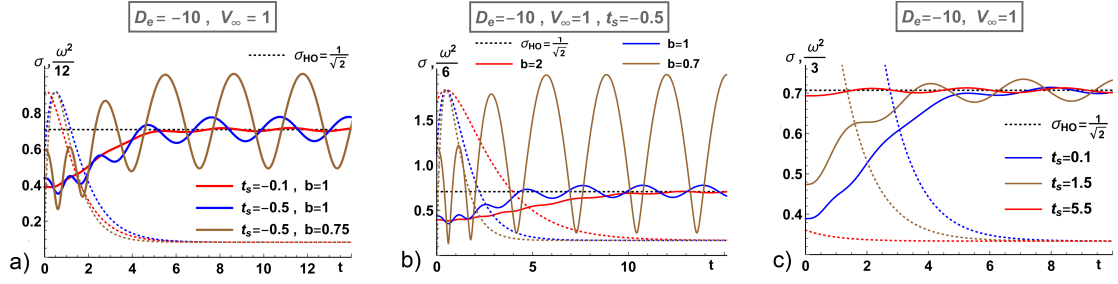


**Figure 5:** Function  $\sigma$  when time translations are performed with  $t_s \neq 0$ . Colored dotted curves refer to scaled  $\omega^2$ . Oscillations of different magnitude are generated depending on the properties of the acting parametric driving.

in altering the evolution trend that the amplitude  $\sigma$  is already experiencing. That is, the system is led in a relatively short time and exponentially fast to a dynamic regime governed by a hamiltonian that is essentially harmonic, with wide amplitudes surviving. If one looks at the envelope profile surrounding oscillations, its modifications are just as adiabatic as expected by comparison with the parametric frequency  $\omega$ .

The case  $t_s > 0$  can be finally commented by noticing that as long as  $t_s$  begins to increase the oscillations tend to become more extensive, but for sufficiently large  $t_s$  the opposite trend is engaged owing to the progressive diminishing of  $\omega_0^2$  (which gets closer to  $V_\infty$ ) and of  $\dot{\omega}$ .

#### 4.3. Case 3: $D_e, V_\infty > 0$

We now consider the standard Morse potential with a positive vertical shift, that is (16) with both  $D_e$  and  $V_\infty$  positive constants, and such to guaranteeing that also the minimum  $\omega_{min}^2$  of  $\omega^2$  is positive:  $0 < D_e < V_\infty$  when  $t_s \leq 0$ , otherwise  $0 < D_e < V_\infty(2e^{-t_s/b} - e^{-2t_s/b})$ . The case is a dual counterpart to Case 2, to which it is linked by a reflection of the  $\omega^2$  shape about the horizontal line identified in terms of the asymptotic value  $V_\infty$ . There is however a difference that has to be accounted for: at fixed  $V_\infty$  and  $D_e$ , quite fast initial variations of parametric frequency may happen when  $t_s < 0$ . Indeed,  $\omega^2$  starts from an initial value  $\omega_0^2$  which, by decreasing  $t_s < 0$ , first keeps itself comparable to the minimum value attained by  $\omega^2$  for small  $t_s < 0$ , then approaches the other reference value  $\omega_\infty^2$ , and later can become arbitrarily great. Magnitude of oscillations for  $\sigma$  is hence expected to not follow an uniform trend while right-translating the curve for  $\omega$  from the  $t_s = 0$  position.

Let us consider the case  $t_s = 0$ . The increasing of  $\omega^2$  from its initial value  $V_\infty - D_e$  means that some energy is pumped into the system, and the evolution of quantities of dynamical interest reflects the presence of such basic mechanism. When  $t_s = 0$  the function  $\sigma$  exhibits an asymptotic oscillating shape that is more and more suppressed as long as the difference  $V_\infty - D_e$  increases, the average values also lowering; see Fig. 6.a). Fluctuations are of greater magnitude whenever  $V_\infty$  and  $D_e$  are comparable. This happens because of the higher value of the initial value for  $\sigma$  along with the wider gap between the initial minimum and the asymptotic value for  $\omega^2$ , the latter giving rise to a less adiabatic dynamics. For sufficiently great values of  $V_\infty$ , the curve obtained for  $\sigma$  essentially flattens, as consequence of the progressive disappearance of the initial hole and of valuable rate changes for  $\omega^2$ .

The picture clearly modifies if the  $\omega^2$  shape previously ruling the dynamics is shifted either to the right or to the left in the  $(\omega^2, t)$  plane, Figs. 6.b) and 6.c). Consider first the case  $t_s < 0$ . With the increasing of  $|t_s|$  keeping  $D_e, b, V_\infty$  fixed, the initial value of function  $\sigma$  diminishes, lessening the amplitude of oscillations maintained in the course of evolution. It is pretty clear, however, that distinguished situations can be expected depending on the magnitude of  $t_s$ . Indeed, for sufficiently small  $t_s < 0$ , the overall qualitative dynamics tailors pretty much to the  $t_s = 0$  case: the initial decreasing trait introduced for the parametric frequency only acts on quite a short time window and the difference between curves' fluctuations at later times (i.e. when  $\omega^2$  approaches its asymptotic value  $V_\infty$ ) is slightly reduced by comparison with the commencing gap  $\sigma(-t_s) - \sigma_0$  (recall that now the minimum  $\omega_{min}^2 = V_\infty - D_e$  for  $\omega^2$  is at  $t = -t_s > 0$ ). While lowering further the value of  $t_s$ , the first part of the amplitude curve goes down and larger fluctuations appear. So, for sufficiently small negative  $t_s$  the magnitude of  $\sigma$  fluctuations reduces compared to the  $t_s = 0$  case, and it increases as expected only later for smaller negative  $t_s$ . Besides, we checked that, by diminishing  $t_s$  further, fluctuations invert few times again the tendency to vary magnitude monotonically, until for sufficiently low  $t_s$  the part

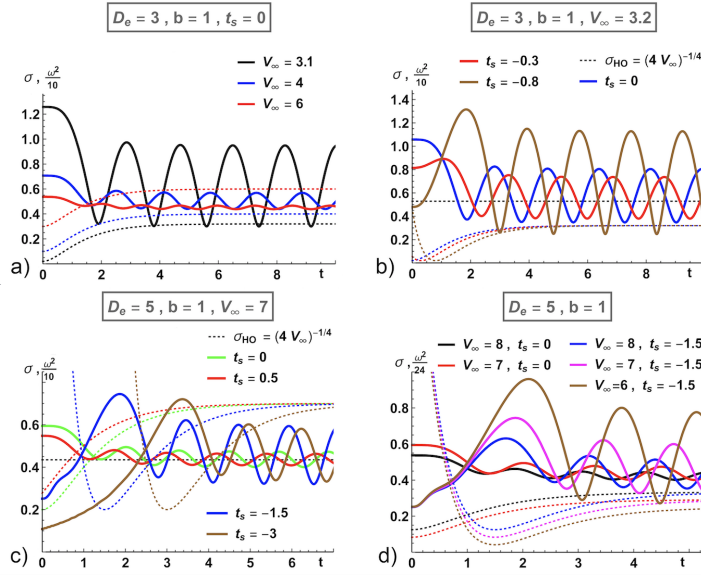


**Figure 6:** Examples of amplitude  $\sigma$  for  $D_e > 0$  and  $V_\infty > 0$ . Initial conditions are (10) with  $c = 1/4$ . Colored dotted curves refer to corresponding scaled  $\omega^2$ . Oscillations of different magnitude are generated by variation of the parameters determining the time-dependent frequency driving.

of  $\sigma$  with regular oscillations appear to freeze and simply translates with the almost constant part of the parametric frequency. These evident changes in the behavior trends seem to be very peculiar of the case under consideration in this Subsection, for which appears a different progression of the competing effects between the jumps taking place between the initial, the extremal and the asymptotic values attained by frequency by monotonic changes of the driving parameters. The waxing and waning mechanism way can indeed be easily checked out by looking how orbits in space  $(\sigma, \dot{\sigma})$  would flow due to changes of the initial conditions implicated for the Ermakov equation.

Vertical translation of the  $\omega^2$  curve towards the time axis augments the magnitude of  $\sigma$  fluctuations. Notwithstanding it may result in a minor variation for  $\omega_0^2$  (and hence  $\sigma_0$ ), a change in the asymptotic value  $V_\infty$  importantly alters the evolution of solutions to the Ermakov equation for quasi normal amplitude  $\sigma$ . Figures 6 show that the effect is really worthy of attention. For instance, in examples shown in graphics 6.d) with  $t_s < 0$ , the asymptotic value  $V_\infty = 7$  is translated by a factor that is only  $1/7$  of its value, but the relative changes in magnitude of oscillations for  $\sigma$  are greater as a consequence of having either halved or increased by 50% the jump  $\omega_\infty^2 - \omega_{min}^2$  (initial decreasing traits for the parametric frequency and jumps  $\omega_0^2 - \omega_{min}^2$  are on equal footing because the  $\omega_0$  experience a percentage variation that are less than 1%). Figures 6.b)-6.d) clearly indicate also that oscillations develop, once again, not symmetrically with respect to the reference amplitude  $\sigma_{HO} = (c/V_\infty)^{1/4}$  associated with the harmonic oscillator whose frequency is the asymptotic value  $\omega_\infty = \sqrt{V_\infty}$  of parametric frequency  $\omega(t)$ . What happens instead when the time shift parameter attains positive values  $t_s > 0$  is very comprehensive: the hole for  $\omega^2$  tends to progressively disappear and the initial value  $\omega_0^2$  assumes higher values, thereby implying for  $\sigma$  that oscillations of smaller magnitude are realized about  $\sigma_{HO}$ .

Figures 6, as well as Figs. 4 provided dealing with Case 2, show an evident consistency with the Sturm theorem, in that the curves  $\sigma$  resulting for majorant  $\omega^2$  possess (in a sufficiently large time interval) more extrema. Even though the concrete examples we explicitly reported by specifying numerical values for the parameters involved are such that the resulting parametric frequency  $\omega^2$  are relatively similar and the effect may not be marked, they still reveal that the frequency of occurrence for the maxima/minima exhibited by the quasi-normal mode amplitude  $\sigma$  does respond to the introduction of majoring/minoring the pumping mechanism for the parametric oscillator (11). In figure 5.a), for instance, effects of the different number of maxima for  $Ax_1^2 + Cx_2^2 + 2Bx_1x_2$  in Eq. (13) are already visible in few time units through an increasing dephasing that is realized. The dynamics of the harmonic oscillator with the minimum value attained by parametric frequency introduces some limits on the oscillation mechanism for the solution to the parametric oscillator equation with the Morse-based frequency (16). From the Sturm comparison theorem

follows indeed that a zero for the parametric equation with the frequency (16) occurs between two successive zeros of solutions to the harmonic oscillator with the asymptotic frequency  $\omega_\infty = \sqrt{V_\infty}$  (Case 2) or  $\omega_{\min} = \sqrt{V_\infty - D_e}$  (Case 3).

We conclude this Subsection by calling attention of the fact that variations of  $b$  has not explicitly argued since the issue can be in effect concluded on the grounds of what we have understood previously.

#### 4.4. Case 4: $D_e > 0$ and $V_\infty < 0$

The Morse-type structure (16) can be finally considered with  $D_e > 0$ , and with a negative vertical shift  $V_\infty < 0$ . In order to avoid  $\omega^2 < 0$ , the case has to be concerned with suitable negative shifts of time variable  $t_s < -b \log(1 + \sqrt{1 - V_\infty/D_e})$  and dynamics over finite time intervals. The case regards therefore a parametric frequency starting from a positive value at initial time, and then monotonically decreasing very rapidly until it vanishes at a certain time (recall Figure 1 and Footnote 1 at page 7). Inspection of the independent solution to the parametric oscillator equation shows a possible generation of initial zeroes and a rapid transition to the exponential growth regime. Once one looks at function  $\sigma(t)$ , the evolutionary trend would appear rather similar to what we have seen in Case 1 with  $t_s > 0$ , with quite modest undulations and the maximum reached at the end of evolution. The dissimilar degree of non-adiabaticity in the monotonic decreasing of the driving  $\omega$  for the two cases intervenes at quantitative level. The changes of the parameter  $b$  determining the time-scale for evolution have an impact on the frequency and its decreasing rate for the present case; indeed, while the duration of signal is affected relatively little, differences for the initial value  $\omega_0$  can be noteworthy. The initial value for the amplitude function defined via Eq. (10) substantially cuts down accordingly.

## 5. Quantum variances and uncertainties

### 5.1. Classical and quantum squeezing of orbits

Solutions to equation of motion for the parametric oscillator define curves in the extended phase space  $(q_c, p_c, t)$ , where  $q_c$  and  $p_c$  denote the classical position and momentum dynamical variables. The collection of all possible orbits in such space that are compatible with an assigned value  $I_{cl}$  of the classical Ermakov invariant (i.e., Eq. (4) with  $q \rightarrow q_c$  and  $p \rightarrow p_c$ ) spans a surface that has the topology of a cylinder. This surface is essentially determined by the classical Ermakov invariant  $I_{cl}$  which, at any given time, defines an elliptic curve in the position-momentum space that collects all the possible pairs  $(q_c, p_c)$  obtained by variation of initial conditions for the Ermakov amplitude equation. During the course of evolution the invariant  $I_{cl}$  generates different ellipses about the origin in the plane  $(q_c, p_c)$  because the functions  $\sigma$  and  $\dot{\sigma}$  vary. These ellipses are of fixed area  $\frac{\sqrt{c} \pi}{16m} = \frac{\pi m I_{cl}}{\sqrt{c}}$  but with foci placement, eccentricity, axes, and length changing in time. Their motion can be schematically be ascribed to variations of quantities  $\sigma$  and  $\dot{\sigma}$ . In particular, defining

$$\delta = \frac{\sigma \dot{\sigma}}{\sqrt{c}} \quad (19)$$

for convenience, intersections of ellipses with axis in phase space  $(q, p)$  are identified via  $q_{c,\pm}^* = \pm \sqrt{I_{cl}} \sigma / \sqrt{c(1 + \delta^2)}$  and  $p_{c,\pm}^* = \pm m \sqrt{I_{cl}} / \sigma$ . The identification of the classically accessible region in phase space put a basis for the connection between classical and quantum aspects of the parametric oscillator dynamics, which is rather naturally validated within a coherent-states approach, where dynamical reshaping of the elliptic sets collecting all couples of position-momentum coordinates that can be realized classically at each time is conveyed at the quantum level to the Wigner ellipses (standard Wigner ellipses result upon replacements  $q_c \rightarrow q_c - \langle q \rangle$  and  $p_c \rightarrow p_c - \langle p \rangle$  in the Ermakov invariant, which is set to the value  $\hbar/2m$ ). Indeed, the coefficients of the quadratic invariant  $I_{cl}$  can be rephrased as second statistical momenta for the position and momentum operators. Precisely, by expressing these operators as linear combination of the operators  $a(t)$  and  $a^\dagger(t)$  through inversion of Eq. (5), it is promptly seen that their variances over Lewis-Riesenfeld coherent and number states,  $|\alpha\rangle$  and  $|n\rangle$ , take the form

$$\Delta_\alpha q = \sqrt{\frac{\hbar}{2m}} \frac{\sigma}{c^{1/4}}, \quad \Delta_\alpha p = \sqrt{\frac{\hbar m}{2}} \frac{c^{1/4}}{\sigma} \sqrt{1 + \delta^2}, \quad \Delta_n q = \sqrt{1 + 2n} \Delta_\alpha q, \quad \Delta_n p = \sqrt{1 + 2n} \Delta_\alpha p, \quad (20)$$

yielding to the Heisenberg uncertainties  $\Delta_\alpha q \Delta_\alpha p = \frac{\hbar}{2} \sqrt{1 + \delta^2}$  and  $\Delta_n q \Delta_n p = \left(n + \frac{1}{2}\right) \hbar \sqrt{1 + \delta^2}$ . The quantity  $\hbar \delta = \hbar \sigma \dot{\sigma} / \sqrt{c}$  can be thus recognized as twice the position-momentum correlation among Lewis-Riesenfeld coherent

states  $|\alpha\rangle$ ,  $\langle\alpha|qp+pq|\alpha\rangle - 2\langle\alpha|q|\alpha\rangle\langle\alpha|p|\alpha\rangle = \hbar\delta$ , and as  $2(1+2n)^{-1}$  times the position-momentum correlation among Lewis-Riesenfeld number states.

Having already scrutinized the behavior of the amplitude  $\sigma$ , to complete gaining insight on the transfer at quantum level of the squeezing dynamics for classical Ermakov ellipses we shall provide examples that outcome for the function

$$\Delta_{UP} = \frac{\hbar}{2} \left( \sqrt{1 + \delta^2} - 1 \right) \quad (21)$$

measuring the deviation from the stationary frequency case of the position-momentum Heisenberg uncertainty over coherent and number states. Results of previous Section for quasi-normal mode amplitudes  $\sigma$  provide a first glimpse in respect to possible evolutions for  $\delta$  and  $\Delta_{UP}$ . Withal, we can notice that the Ermakov equation can be managed to generally write  $\sqrt{c}\dot{\sigma} = (c - \omega^2\sigma^4)\sigma^{-2} + \sigma^2 = [(c - \omega^2\sigma^4) + c\delta^2]/\sigma^2$ , that gives an indication about the way the degree of adiabaticity of amplitude  $\sigma$  changes can act in squeezing Ermakov-Wigner ellipses and build up nontrivial correlations in the course of system's evolution. We thus expect that in some cases deviation of products  $\Delta_{\alpha q} \Delta_{\alpha p}$  cannot be neglected compared to the familiar minimum value  $\hbar/2$ .

## 5.2. Position-momentum uncertainties. Case 1: $D_e, V_\infty < 0$

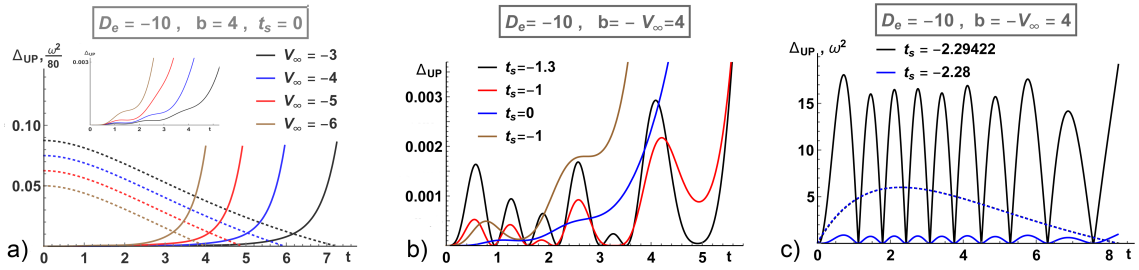


**Figure 7:**  $\Delta_{UP}$  in  $\hbar = 1$  units when  $\omega(t)$  is given via Eq. (16) with  $D_e, V_\infty < 0$ . a) Examples with fixed  $D_e, b$  and  $t_0 = 0$  and varying  $V_\infty$ . The plot in the upper corner gives a close-up of initial trait of the curves. b) Initial traits of curves  $\Delta_{UP}$  obtained with positive, vanishing and negative values of  $t_s$ . c) Generation of large fluctuations when  $t_s < 0$ . Dotted curves refer to parametric frequencies generating the  $\Delta_{UP}$  plotted with solid lines of the same color (overlapping in last plot).

Assuming the initial conditions (10), the quantity (21) is vanishing at initial time. Main aspects concerning what happens after that time are shown in Figure 7. They can be subsumed as follows. When  $t_s = 0$  the growth of  $\Delta_{UP}$  is fairly smooth and slow, before to raising markedly in the final course of dynamics as the time (18) is going to be approached. In Figure 7, for instance, the maximum gain for  $\Delta_0 \hat{q} \Delta_0 \hat{p}$  is a bit below 20% of its initial value. Lowering the parameter  $V_\infty$ , the pumping mechanism operates on a shorter time interval and  $\Delta_{UP}$  varies faster. If  $t_s$  is varied from zero, forewarning of oscillations begin to arise. The generation of a succession of peaks is distinct when  $t_s < 0$ , which is the case where a sign change is experienced by  $\dot{\omega}$ . The lowering of  $t_s$  makes the oscillating pattern more uniform, but also of greater magnitude as the shape of the frequency parameter  $\omega$  varies more before the maximum is reached at  $t = -t_s$ . When  $\omega_0$  gets very close to zero, minor variations of  $t_s$  leading to inappreciable variation of the frequency parameter shape obviously provoke impressive alteration for the magnitude of oscillations; in Figure 7.c), this is shown with values for the maxima of  $\Delta_{UP}$  that jump at great rate from about  $\hbar$  to more that 15 times that value.

## 5.3. Position-momentum uncertainties. Case 2: $D_e < 0$ and $V_\infty > 0$

Once again, the position-momentum Heisenberg uncertainty may depart pretty much from the stationary result. The effect may be sustained in the course of dynamics, or first and foremost confined at early stages when frequency changes are more gradual. Figures 8 are obtained by varying parameters  $b$  and  $t_s$ . Figure 8.a) shows examples where  $b$  is small and peaks of  $\Delta_{UP}$  range from about 10% to 80% of the initial uncertainty value  $\hbar/2$ . In Figure 8.b) the parameter  $b$  that scales the time variable  $t$  is increased and magnitude of  $\Delta_{UP}$  falls off consistently. A transient initial dynamics is clearly seen, especially for  $t_s \neq 0$ , where the largest contributions to the position-momentum uncertainty are recorded (not exceeding 2% of  $\hbar/2$  with parameter used in Fig. 8.b) ).



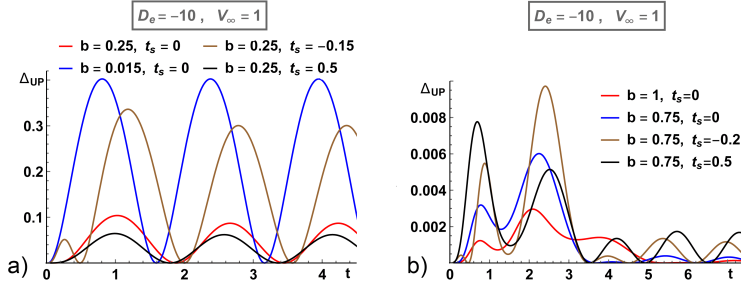


**Figure 8:** Examples of  $\Delta_{UP}$  curves in  $\hbar = 1$  units when  $V_\infty > 0$  and  $D_e < 0$  in (16).  $D_e$  and  $V_\infty$  are hold fixed while there are two different varying sets for  $b$  and  $t_s$ . Smaller values of  $b$  amplify the deviation from minimal Heisenberg uncertainty  $\hbar/2$  and hide initial transient effects.

#### 5.4. Position-momentum uncertainties. Case 3: $D_e > 0$ and $V_\infty > 0$

Even when both  $D_e$  and  $V_\infty$  in (16) are positive constants, amplitude fluctuations may generate oscillating enhancements of the Heisenberg uncertainty for certain values of parameters determining the shape of frequency parameter. Examples are given in Figure 9.a) with parameters that make the effect standing out. The increasing of  $V_\infty$  at fixed  $D_e$  suppresses responses for  $\Delta_{UP}$ . When  $t_s$  decreases from the null value, a damping of the  $\Delta_{UP}$ -oscillations first results that is next replaced by the foreseen amplification trend. Relatively limited reshaping of the parametric driving can result in evident changes for magnitude of oscillations; see red and blue curves in both panels of Figure 9. As we learned Subsection 4.3, the proximity to the null value of initial frequency value is indeed a crucial matter.

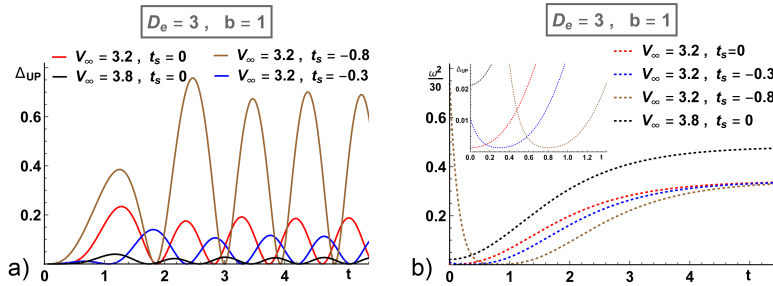


**Figure 9:** Case 3:  $D_e, V_\infty > 0$ . a) Oscillations generated for  $\Delta_{UP}$  in  $\hbar = 1$  units. b) Scaled  $\omega^2$  relative to examples in a).

We do not present figures for Case 4, for which we found curves for  $\Delta_{UP}$  that resemble those of Fig. 7.a) of Case 1 but with a marginal indication of an underlying fluctuation mechanism before the final fast growth.

## 6. Zero-delay second order correlation functions

For investigating the evolution of a quantum field governed by a time dependent quadratic hamiltonian, it is convenient to construct either the eigenstates of the time-dependent annihilation operator or those of the time-dependent number operator, and to connect them to the standard coherent and number states for the harmonic oscillator identified by factorization of the hamiltonian at an initial time. This allows to realize a description of the dynamics based on Lewis-Riesenfeld coherent- or number-type states, and to interpret the results in terms of stationary coherent states or modal excitations constructed through a diagonalization of the Hamiltonian at some initial time. Features of the eigenstates of  $I$  are intimately connected to those of eigenstates of the harmonic oscillator with mass  $m$  and frequency  $\omega_0$  because of the extended canonical transformation linking each to the other (Section 2), but they present specific peculiarities induced by the concrete form of the transformation, i.e. the vacuum state actually considered. The probability of finding an element from the modal Fock basis  $\{|n\rangle_0\}$  in a Lewis-Riesenfeld squeezed coherent state  $|\alpha\rangle$  does not follow a Poisson distribution. Related to the mechanism of time-dependent squeezing of quadrature components, modifications of modes counting statistics are manifested during the evolution of the one-mode quantum system governed by a parametric oscillator hamiltonian operator. They can be highlighted by determining the values of the the

second-order degree of coherence [46]. In this Section we shall therefore analyze the zero-delay correlation functions

$$g_2 = \frac{{}_0\langle n|\hat{a}^\dagger{}^2\hat{a}^2|n\rangle_0}{{}_0\langle n|\hat{a}^\dagger\hat{a}|n\rangle_0^2} = \frac{{}_0\langle n|N^2|n\rangle_0 - {}_0\langle n|N|n\rangle_0^2}{{}_0\langle n|N|n\rangle_0^2}. \quad (22)$$

The function  $g_2$  can be determined on purely algebraic grounds on account of the Bogolubov mapping (6) with (9), yielding to

$${}_0\langle n|N|n\rangle_0 = n + (1 + 2n)|v|^2, \quad (23)$$

$${}_0\langle n|N^2|n\rangle_0 = n^2 + 2(3n^2 + 2n + 1)|v|^2 + 3|v|^4(2n^2 + 2n + 1), \quad (24)$$

so that

$$g_2 = \frac{n(n-1) + (6n^2 + 2n + 1)|v|^2 + 3|v|^4(2n^2 + 2n + 1)}{[n + (1 + 2n)|v|^2]^2}. \quad (25)$$

The creation of modes out of a state (e.g. the vacuum) is determined by the square modulus of the Bogolubov coefficient  $v$ . At early stages of dynamics the process follows a power-law with scale exponent determined on account of initial conditions superimposed to  $\sigma$  and  $\dot{\sigma}$ , and of initial values for parametric frequency and its t-differentials. Working with Lewis-Riesenfeld invariant number states based on the minimal uncertainty conditions (10), one has  $|v(t)|^2 \simeq \frac{\sqrt{c}}{4\omega_0\sigma_0^2}\dot{\omega}_0^2 t^4 + h.o.t.$  if  $\dot{\omega}_0 \neq 0$  and  $|v(t)|^2 = \frac{\sqrt{c}\dot{\omega}_0^2}{36\omega_0\sigma_0^2}t^6 + h.o.t.$  if  $\dot{\omega}_0 = 0$ , the approximate form for the leading correction

to zero delay correlation function  $g_2$  following accordingly via  $g_2 \simeq 1 - \frac{1}{n} + \frac{2n^2+4n+3}{n^2}|v|^2$ . For the problem under consideration in this communication, in particular, the distinction relies on the value for time-translation parameter  $t_s$  in (16) since  $\dot{\omega}_0 = 0$  for  $t_s = 0$ . Once it is assumed that minimal uncertainty is realized at initial time for elements of the invariant Fock space owing to (10), the initial variance of the invariant number operator is vanishing and the initial value for correlation function  $g_2$  is the standard  $1 - 1/n$  (with  $n \neq 0$ ) associated with the harmonic oscillator.

### 6.1. Case 1: $D_e, V_\infty < 0$

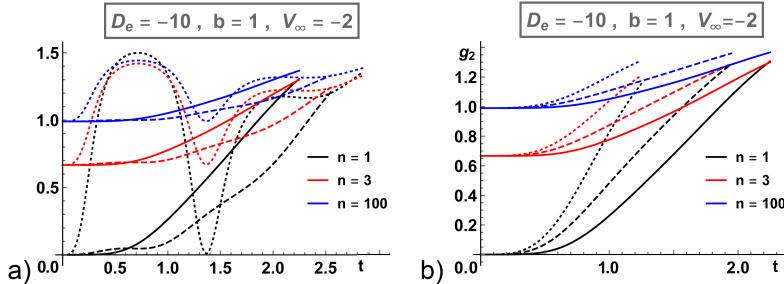


**Figure 10:** Second-order correlation functions (22) evaluated over  $|n\rangle_0$  with  $n = 1, 3, 100$ , Eq. (25). Left panel:  $t_s = -0.6$  (dotted),  $-0.3$  (dashed),  $0$  (solid); Right panel:  $t_s = 0$  (solid),  $0.3$  (dashed),  $1$  (dotted). When  $t_s < 0$  substantial deformations of  $g_2$  curves originate and switches between sub- and super-poissonian regimes are realized.

In general, for fixed frequency parameters the curves for  $g_2$  assume higher values by increasing the occupation number  $n$ . Figures 10 subsume the essential features displayed when one is concerned with a parametric frequency associated with the case, Eq. (16) with  $D_e, V_\infty < 0$ .

If  $t_s = 0$ , there are no signs of undulations. The system starts to evolve from an adiabatic condition and initial variations of frequency parameter  $\omega$  do not affect much the 2-point correlation function. But after a certain time  $g_2$  begins to increase its values almost linearly until reaching its maximum at the final time  $t_+$ , Eq. (18). So there is a mechanism acted by the driving parametric frequency that steadily directs the sub-poissonian initial statistics to a super-poissonian one eventually. Needless to say, for the occupation number  $n = 1$  state the process is longer, but when the memory of adiabatic initial condition is lost the rate of growth is noticeably higher than for other number states. Such rate decreases with the increasing of the occupation number, albeit very soon the differences become insignificant. At

the final time values for  $g_2$  group closely. Figures 10 also show what happens whenever a shift of the frequency curve is performed by means of translations of time variable. For positive shifts  $t_s$  the time interval where dynamics takes place is shorter, and it turns out that the growing manifests itself with a greater rate but the final maximum value slightly decreases. It goes without saying that for negative time shift parameter dynamical responses for  $g_2$  change. For small negative  $t_s$  there are marks of fluctuations forming. For larger negative  $t_s$  a well defined bell-like profile characterizes  $g_2$ , whose maximum develops about the time  $t = |t_s|$  when the parametric frequency displays its extremum. The top of the bell is in the  $g_2 > 1$  portion of the plane, and hence it is concerned with super-poissonian characteristics. A dip follows that drives the statistics to sub-poissonian regime for a short time interval (getting shorter with the increasing of the occupation number), unless one is concerned with rather high occupation numbers (with parameters of figure 10.a) and  $t_s = -0.6$  one gets  $n > 422$ , for instance). A renewed propensity to increase bunching follows guiding back to super-poissonian features, followed by another change of signs for differentials of minor extend.

What happens by varying the intensity of the Morse term when  $t_s < 0$  is shown in graphics 11. Curves tend to lower or uprise as a consequence of changes in initial condition and time-window for dynamics. Higher values of  $D_e$  result in the enlargement of the bell, and in the replacement of the maximum peak with a bigger and bigger plateau. In contrast, lower values of parameter  $D_e$  introduce more oscillation of lower magnitude, and hence more changes in the statistics. For  $t_s > 0$ , one would see instead that the decrease of  $D_e$  merely tends to lowering curves 10.b) and spreading them in a wider time interval.

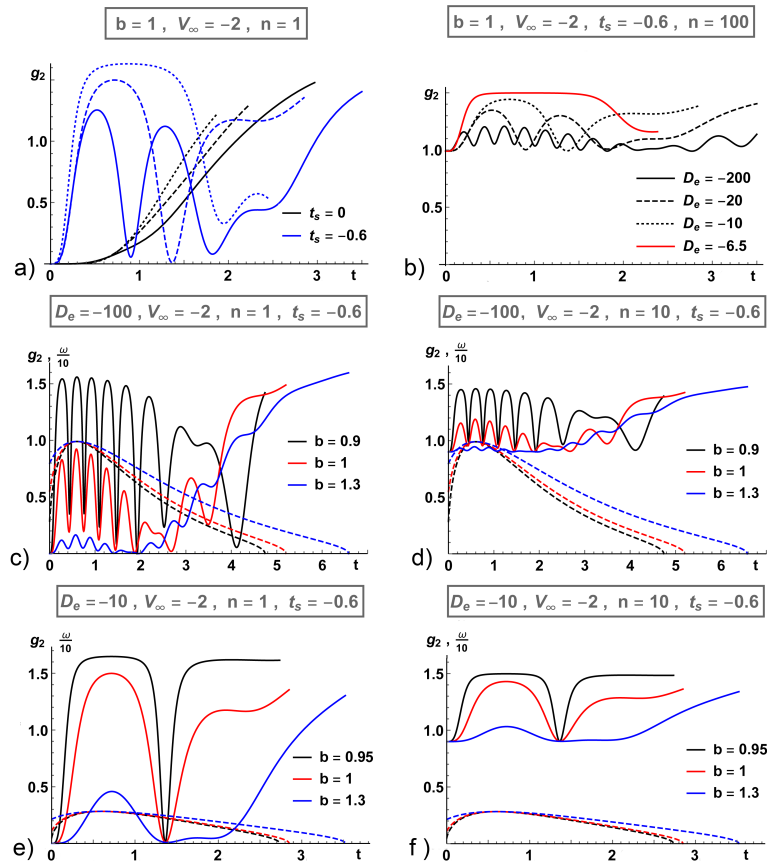


**Figure 11:** Case 1: second-order correlation functions evaluated over harmonic oscillator eigenstates. a)  $n = 1$  and  $D_e = -20, -10, -7$  (solid, dashed, dotted); b)  $n = 10$ . By adjusting the frequency parameters, essential changes affect the particle creation mechanism and remould  $g_2$ , with more squared shapes or more peaks emerging, or with suppression/amplification of fluctuations. For low quantum numbers, inverted spikes can be seen due to the sudden changes in the dynamics.

It is now important to see what happens by refining the parameter  $b$  which fixes the scale for the time-evolution parameter  $t$ . The operation really has a repercussion on the determination of  $\omega_0$ , and of adiabaticity of  $\omega$  and  $\sigma$ . Indeed,

we can see that the dynamics of correlation functions  $g_2$  contrasts dramatically with that comprehended previously for  $b = 1$ . For higher values of  $b$ , the adiabaticity of the driving improves:  $\omega_0$  approaches the maximum value of  $\omega(t)$ ; in addition, the parametric frequency curve stretches out on a wider time domain, Eq. (18). The initial prominence previously seen for the correlation function  $g_2$  is appreciably dampened, and the successive going up again is evidently done much less quickly. In contrast, for lower values of  $b$ , the previously observed initial bell-like shape turns into a more squared profile, with the formation of a second plateau. The role  $b$  has in suppression or enhancement of sudden changes is obviously lead to situations based on different choices for the other parameters defining the frequency parameter. In particular, we have already noted through Figs. 11.a) and 11.b) that lowering  $D_e$  introduces more fluctuations for the correlation function, though with lessened magnitudes. Figures 11.c) and 11.d) present what results if a variation for  $b$  is performed in combination the assumption of large values for  $D_e$ . In these figures,  $D_e = -100$ , rather compressed and wide fluctuations for  $g_2$  are shown that are generated in the first part time evolution for  $b = 1$ , and wider ones, with higher mean values, are sustained once  $b$  diminishes. In the remaining part of evolution, that pattern breaks, to eventually conduct (with or without fluctuations, depending on the case) the function  $g_2$  in the super-poissonian regime. For higher values of  $b$ , the initial oscillations are strongly suppressed and values for  $g_2$  in the first part of dynamics also are much contained. For the second part of evolution a stretching of the  $b = 1$  curve over the enlarged time interval appears.

## 6.2. Case 2: $D_e < 0$ and $V_\infty > 0$ .

Bearing in mind the discussion in Section 4 concerning the amplitude  $\sigma$  dynamics, one is aware beforehand of the incidence of oscillatory features for the parametric oscillator problem when evolution is governed by the pumping mechanism of Cases 2 or 3 defined in the infinite time interval  $t \in [0, \infty)$ . Specifically, translations of the Morse-type curve for  $\omega^2$  are expected to give rise to a gradual developing of oscillation in the  $g_2$  spectrum.

In Figure 12 we have plotted typical curves for the correlation function  $g_2$  that elucidate the various influences of the shift parameter  $t_s$  entering the parametric frequency. If  $t_s = 0$ , an initial augment for  $g_2$  that reminds of that seen in case 1 is followed by a sort of asymptotic saturation with extremely weak signs of fluctuations. When one is concerned with high occupation numbers, a super-poissonian regime is obviously realized in relatively short time. The major differences one has in the initial magnitude of  $g_2$  for the very low occupation numbers vanishes in the course of dynamics, as curves tend asymptotically to attain values in a small domain. Being more attentive to the first trait of the curves, it is seen that the successive minor fluctuations are in fact anticipated by rather unperceivable variations in the rate of the function's growth. So it is intuitive that the case possesses the characteristics for sustaining large oscillations in the  $g_2$  spectra whenever changes are introduced via nontrivial time shifts  $t_s \neq 0$ . If  $t_s < 0$ , pronounced oscillations indeed arise owing to the major degree of non-adiabaticity of frequency variations to which states are subjected in their initial dynamics. A regime of regularity in the oscillator of  $g_2$  appears after a transient time. In the first course of dynamics, the frequency increases to reach its maximum, and a first local maxima is in fact exhibited by  $g_2$  through a peak above the  $t_s = 0$  curve. After this peak, the  $g_2$ 's profile stays below the  $t_s = 0$  curve, but goes towards it oscillating. When sufficient time is passed, the curve for  $g_2$  with  $t_s < 0$  sustains more regular oscillations, whose maxima get close to the  $t_s = 0$  curve. The increasing of the occupation number let the magnitude of shape variations diminish. If  $t_s > 0$ , obviously departures from the  $t_0$  curves are realized to a minor extend. By comparison with plots when  $t_s = 0$ , a bit higher values can be detected in the initial growth of  $g_2$ , and lower ones later on.

It is now interesting to comprehend what happens by refining the time scale where the exponential terms in the frequency act more importantly. In view of findings in Subsection 6.1, we expect appreciable alterations of the previous big picture. Figure 12.b) shows an example on the consequences a scaling  $b \rightarrow b/4$  produces if all the other parameters of figure (12) are unaltered. If we take  $n = 1$  (the case experiencing the greater excursions of values assumed), we can see that large oscillations show up even when  $t_s = 0$ , and  $\dot{\omega}$  vanishes at initial time. Alternation of sub/super poissonian changes occurs. Increasing positive  $t_s$  both the maxima and the magnitude of oscillations progressively reduce, and a damping mechanism acts on the curves. For  $t_s < 0$  a different process operates that in the end spoils fluctuations. For low negative  $t_s$  oscillations actually increase, but later they are inhibited: when  $t_s$  is decreased further, the curve is gradually lifted up to a reference stationary value, reached in very short time. For low negative  $t_s$  the minima attained in the course of oscillation approaches the initial value for  $g_2$ . When  $t_s$  is decreased further, curves  $g_2$  are bounced back. The initial value for  $g_2$  sets a reference bound value also quantum numbers  $n$  are greater than 1, an instance being given in Figure 12.c). As for counting statistics, the parametric driving is capable to imprint an essentially super-poissonian behavior, unless very low quantum occupation numbers  $n$  and monotonically varying frequency  $\omega$  are concerned.

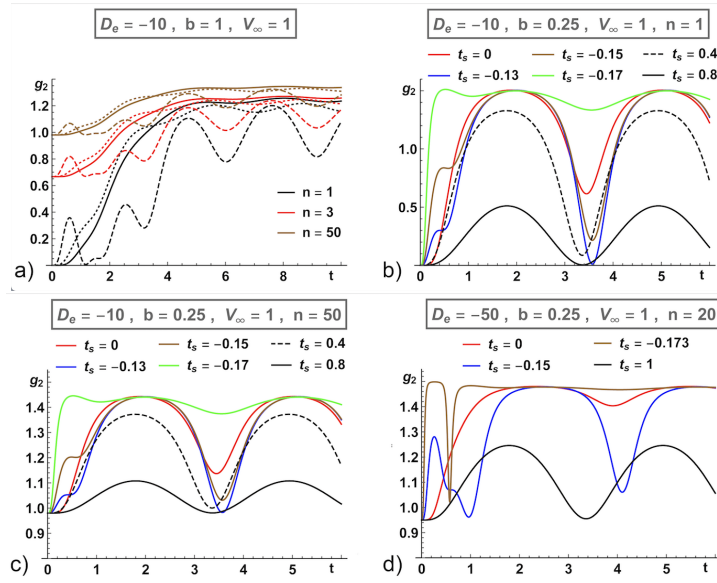


**Figure 12:** Case 2:  $g_2$  over number states. a)  $t_s = -0.5, 0, 0.5$  (dashed, solid, dotted); b)  $n, D_e, V_\infty$  are as in a), but with smaller  $b$  and different  $t_s$ ; c)  $n = 50$  and  $b, D_e, V_\infty$  as in figure b). d)  $n = 20$  and  $b, V_\infty$  as in previous two plots. Figures show oscillation patterns forming after an initial time transient. Oscillation may be as enlarged to reach the initial values and to provoke a bouncing of curves along with reduced minima/maxima excursions, see b)-c). For greater values of  $|D_e|$  an inverted spike is seen to develop for the lowest allowed values of  $t_s$ .

### 6.3. Case 3: $D_e, V_\infty > 0$

Plotting the zero time delay correlation function  $g_2$  versus time we see the expected generation of fluctuating patterns. Figures 13 give the gist of variation of occupation number  $n$  and time-shifts  $t_s$ . The oscillating pattern is flattened down by higher values of positive  $t_s$ , as upshot of the declined initial variation and non-adiabaticity experienced by the parametric frequency.<sup>3</sup> For small negative values of  $t_s$ , one witnesses to a right and down translation of the profile. This mechanism is accompanied by the birth of a new initial hump that, once lower values for  $t_s$  are assumed, it is lifted up with all the others present about the portion of the  $t_s = 0$  curve that attains maximal values. Diminishing further the parameter  $t_s$ , a saturation character emerges: plateau form that are interrupted by the small holes generated by the minimum-maximum excursions traits being suppressed and pushed up.

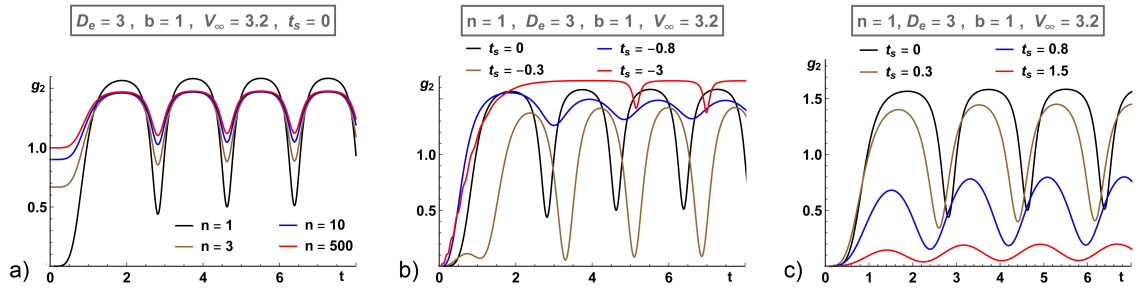


**Figure 13:** Case 3:  $g_2$  over number states. a)  $t_s = 0$  and  $n = 1, 3, 10, 100$ ; b) negative  $t_s$  and  $n = 1$ ; c) positive  $t_s$  and  $n = 1$ . Inverted spikes are introduced in the oscillating pattern that are smoothed out with the increase of the quantum number  $n$  and the tuning of  $t_s$ .

<sup>3</sup>Both in this case and the previous one of Subsection 6.2, Bogolubov coefficients  $\mu_\infty = \frac{\omega_\infty + \omega_0}{2\sqrt{\omega_\infty \omega_0}}$  and  $\nu_\infty = \frac{\omega_\infty - \omega_0}{2\sqrt{\omega_\infty \omega_0}}$  referring to an adiabatic asymptotic limit may be introduced to approximately assess at the lowest order the modification of statistics at large times.



#### 6.4. Case 4: $D_e > 0$ and $V_\infty < 0$

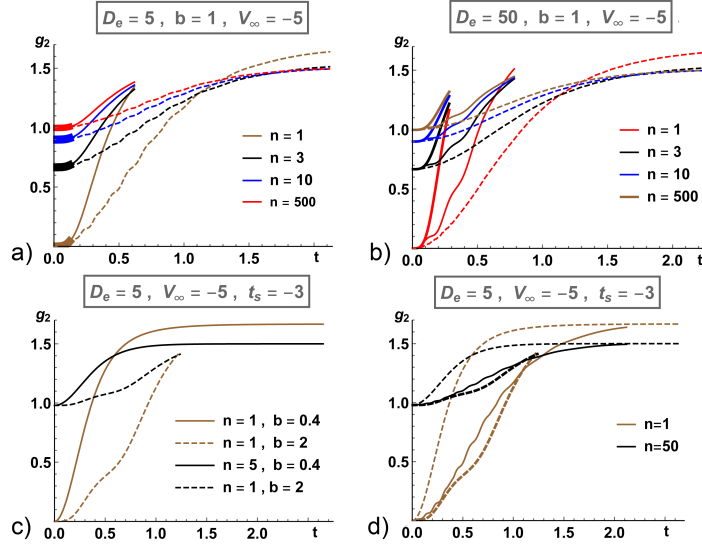


**Figure 14:** Examples of  $g_2$  over number states in Case 4 for different parametric frequencies. a)-b)  $b = 1$ ,  $V_\infty = -5$  and  $t_s = -1, -1.5, -3$  (solid thick, solid, dashed);  $D_e = 5, 50$ . c)  $D_e = 5$ ,  $V_\infty = -5$ ,  $t_s = -3$ ,  $b = 0.4, 2$  and  $n = 1, 5$ . d)  $D_e = 5$ ,  $V_\infty = -5$ ,  $t_s = -3$ ,  $b = 0.4, 1, 2$  (dashed, continuous, dashed thick) and  $n = 1, 50$ .  $g_2$  is subjected to a fast growing behavior turning into a plateau if the parametric driving is active for sufficiently long time.

The driving mechanism exerted by the parametric frequency now runs for a short time interval (in  $b$  units) and selecting the most rapidly varying portion of the Morse curve. Examples of functions  $g_2$  are provided in Figure 14, showing how they move into the  $g_2 > 1$  region if the system evolves for a sufficiently large time. For intermediate values of negative parameter  $t_s$ , the case it is seen to share some similarities with Case 1 with  $t_s \geq 0$ , Fig. 10.b). The duration of time interval where the driving mechanism is active does not get through  $t_+$ , Eq. (18), creasing limitedly for higher values of  $D_e$  and  $t_s$ . Effects of such an enlarging the time window where the dynamics takes place are visible with possible vague signs of prior undulations, and with an additional trait suggesting that it would likely progress to a saturation. It is the acting on the value of time-scale parameter  $b$  that allows the saturation to take a more concrete form, by simultaneously smoothing the modest undulations. As we have noticed in Subsection 4.4, most influential alterations for the frequency parameter are indeed those of parameter  $b$ , whose reduction gives a notable boost to values for  $\omega_0$  and the rate of changes for  $\omega$ . These then imply a strong suppression of the initial value  $\sigma_0$  that is assumed via (10) for the solution  $\sigma$  to the Ermakov equation, and an enhancement of the variation of  $\sigma$  that can be observed at later times compared to its initial value. This makes a difference because the Bogolubov coefficient  $\nu$  is quite sensitive to quantitative changes experienced by the function  $\sigma/\sigma_0$ . When  $\sigma/\sigma_0$  deviates from values that are close the unity, a growth for  $|\nu|$  is dictated that easily can be sufficient to determine the  $|\nu|^4$  terms dominating  $g_2$ . Under these circumstances, at a certain point the mode creation mechanism can be therefore strong enough to let  $g_2$  approach a quality of stationarity.

## 7. Delayed second order correlation functions

To complete the understanding of statistical aspects we earned so far through the zero-delay correlation functions, it is helpful to considering also the two-time correlation function over states  $|n\rangle_0$ , i.e. the function

$$g_2(\tau) = \frac{{}_0\langle n|a^\dagger(t)a^\dagger(t+\tau)a(t+\tau)a(t)|n\rangle_0}{{}_0\langle n|a^\dagger(t)a(t)|n\rangle_0}. \quad (26)$$

This enables one to get an insight into the fulfillment of anti-bunching/bunching requisites and the possibility to measuring modes in a time-delayed fashion with higher probability than being measured at the same time. We will limit

ourselves to the cases where  $D_e$  and  $V_\infty$  are both either positive or negative (Cases 1 and 3) because they allow to epitomize the basic features displayed also for different choices of the driving frequency parameters. Yet, we shall focus on correlations over the lowest excited states  $|n\rangle_0$  as they present wider domains where anti-bunching is accomplished.

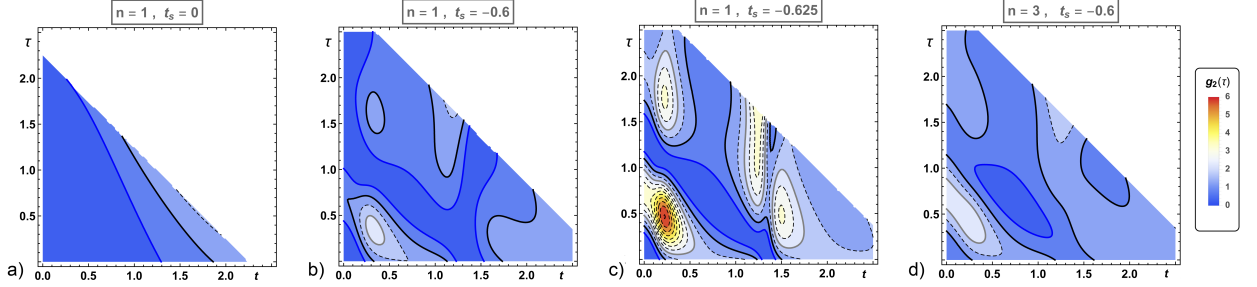


**Figure 15:** Case 1: parametric frequency (16) with  $D_e, V_\infty < 0$ . Level plots for the delayed correlation function  $g_2(\tau)$  when  $D_e = -10$  and  $V_\infty = -2$ . Thick solid curves refer to  $g_2(\tau) = 1/2$  (blue),  $g_2(\tau) = 1$  (black),  $g_2(\tau) = 2$  (gray). a)-c) Dynamics underlying the reduction of anti-bunching and the surfacing of strong bunching when  $n = 1$  and the parametric frequency initial shape is modified by assuming  $t_s = 0, -0.6, -0.625$ . d)  $n = 3$  and  $t_s = -0.6$ ; by comparison with figure b) the effect of changing the reference state is noted.

Plots in Figure 15 provide instances of the bunching and anti-bunching mechanisms possibly realized by considering different time-translation parameters  $t_s \leq 0$  for the parametric frequency (16) with  $D_e, V_\infty < 0$ . Having a finite time interval over which the dynamics takes place clearly introduces a finite domain for the delay variable  $\tau$ . If  $t_s = 0$  and the very low occupation numbers  $n$  are concerned, there is a mostly anti-bunched behavior that is displayed by varying the time  $\tau$  determining the second counting. For  $n = 1$  a relatively vast area denoting strong anti-bunching ( $g_2(\tau) < 1/2$ ) obviously arises, a strong anti-bunching being sustained for all the allowed  $\tau$  for lower  $t$ 's -Fig. 15.a). Diminishing  $t_s$ , the moderate extension of the time domain allowed for evolution causes an enlargement of the region in the  $(t, \tau)$  plane that identifies anti-bunched responses; this also holds for the strongly anti-bunched domain appearing for  $n = 1$ . At this stage, contour plots for  $g_2(\tau)$  thus qualitatively resemble those obtained for  $t_s = 0$ . By diminishing further the values of  $t_s$  so to have less adiabatic initial changes for the parametric frequency and more pronounced fluctuation effects for physical quantities, the picture for second-order correlation functions modifies: islands reflecting bunching phenomena are introduced, possibly tending to connect each to the other while introducing higher values for  $g_2(\tau)$ . Remark that the condition  $t_s < 0$  (which implies a change of sign for  $\dot{\omega}$  at early times) does not exclude the possibility to support the detection of strong anti-bunching  $g_2(\tau) < 1/2$  when  $n = 1$ , even though an overall inclination to build bunched super-poissonian responses may be displayed. Figure 15.b) shows for instance that for  $n = 1$  a strong anti-bunched path can be identified in plane  $(t, \tau)$  that originates when  $t_s$  is about 1.4 and  $\tau$  is varied in its whole allowed domain. For the closely successive values of the quantum number  $n$ , the behavior of correlations  $g_2(\tau)$  is affected accordingly, see Figure 15.d) determined for  $n = 3$  and with the same frequency parameters  $D_e, b, V_\infty$  and  $t_s$  of Figure 15.b). The zero-delayed second order correlation function does not present strongly sub-poissonian traits as in the  $n = 1$  case, but delayed correlation can attain low values. In Fig. 15.d) it is seen that strong bunching or strong anti-bunching can be detected.

When  $D_e, V_\infty > 0$  in (16) there is no upper time limits for the dynamics and regular oscillating patterns generate after the initial transient. These circumstances are reflected in functions  $g_2(\tau)$ , and the tendency to develop repeating patterns is recognized. Figures 16.a)-c) show, in particular, examples referring to the two-time correlations over the states  $|1\rangle_0$ . The alternation of domains associated with strong manifestations of anti-bunching and bunching is visible in Figure 16.a), concerned with a case for which  $t_s = 0$ . Upon decreasing the parameter  $t_s$  patterns modify, a suppression on responses takes place and larger islands associated with anti-bunching show up for  $\tau > 0$ , Fig. 16.b). By further decreasing  $t_s$  the foreseen reinforcement for the mechanism of bunching follow, Fig. 16.c), with higher values for  $g_2(\tau)$  attained by increasing the quantum number  $n$ , Fig. 16.d).

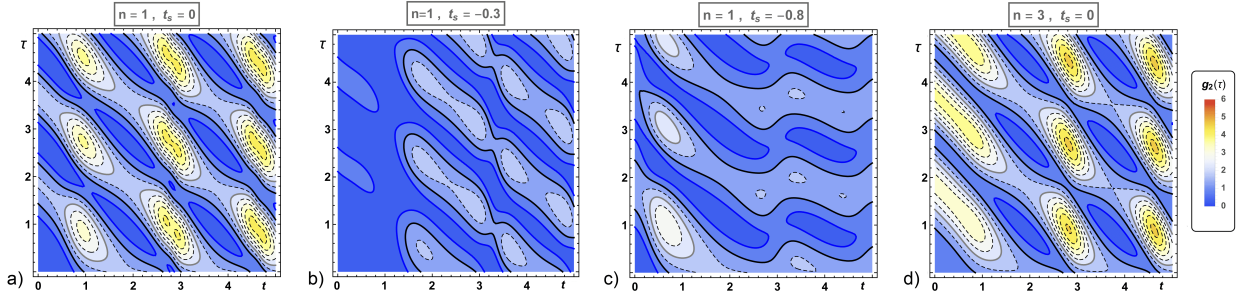


**Figure 16:** Case 3: parametric frequency (16) with  $D_e, V_\infty > 0$ . Level plots for the Glauber function  $g_2(\tau)$  over number states  $|n\rangle_0$  when  $D_e = 3$  and  $V_\infty = 3.2$ . Thick solid curves refer to  $g_2(\tau) = 1/2$  (blue),  $g_2(\tau) = 1$  (black),  $g_2(\tau) = 2$  (gray). a)-c) Revival and collapse of bunching and antibunching when  $n = 1$  and the parametric frequency initial shape is modified by assuming  $t_s = 0, -0.3, -0.8$ . d)  $n = 3$  and  $t_s = -0.8$ ; by comparison with figure c) the effect of changing the reference state is noted.

## 8. Conclusions

We have discussed the dynamics of one-degree of freedom Hamiltonian of the parametric oscillator type with a time-dependent frequency based on a Morse potential shape, up to possible translation and sign reversion. This provided us an analytical framework to examine both cases where there is a monotonic increasing or decreasing energy pumping mechanism, and cases where there is an alternance of them realized continuously. Depending on choices of the parameters, the pumping mechanism can be active unlimited or cease after a certain time interval.

For time-dependent quadratic systems, solution to the Schrödinger equation and quantum dynamics are manifestly based on classical dynamics as the centroid and the spreads of a wave-packet follow exactly the evolution of a classical particle [34, 35, 36, 37]. We thus detailed (Appendix A) the derivation of solution to classical equation of motion for the parametric oscillator with the time-dependent frequency we set out and (Section 4) analyzed the features of their amplitudes  $\sigma$ , whose variations are governed by the Ermakov nonlinear differential equation and direct all the dynamical consequences. Enhancement and suppression of their oscillations by virtue of frequency parameter shape changes have been thoroughly inspected, with plots summarising the behavior of functions  $\sigma$  for different values of the parameters involved and the initial conditions we adopted for the Ermakov differential problem (1). Figures show, for instance, the manner Sakharov-type regular oscillatory patterns in systems' responses do form when the parametric frequency modifies to eventually approach a quality of stationarity. They also illustrate how, when initial conditions and the changes for the parametric driving are such that a big (non-adiabatic) effort is needed for the system to adapt itself to the dynamical circumstances, larger oscillation develop about the leading order curve from the WKBJ expansion method. Progressive enlargement of fluctuations for non-adiabatic changes of amplitudes  $\sigma$  adapt closer and closer to (the absolute value of) the complete non-stationary mode solutions to the parametric oscillator equation; accordingly, the phases  $\theta(t)$  of classical modes develop by alternating sudden continuous jumps to nearly constant traits, a behaviour inherited at the quantum level by the geometrical phases (3).

We later argued on how quantum dynamics mirrors the squeezing mechanism implied at the classical level on the Ermakov invariant orbits on phase-space, and in this respect we presented plots related to the Heisenberg uncertainty relation on number-type and coherent-type states, including some examples showing that these uncertainties can act on a scale greater than  $\hbar$ . Finally, to refine the insight into the statistical contents implied, the generation during the course of evolution of nonclassical features for number-type states has been discussed by investigating deviation from Poisson statistics of two-point correlation function with zero time delay owing to the squeezing dynamics taking place. Delayed two-point correlations have also been considered to attest the phenomena of time-depending bunching and anti-bunching showing up. Results obtained clearly show trends of collapse and revival phenomena whose intensity is conditional on the dynamical facets that have been highlighted for the solution to the Ermakov equation.

Studies like the one we performed in this communication find a natural arena of application, e.g., within the context of the electromagnetic wave propagation in time-dependent media [2, 29, 30, 3, 4]. The analysis can be then continued by taking into account more complicated states or by implementation of quasi-probability tools. In particular, linear combination of states can be considered to analyze the competition between interference effects and parametric

frequency variations both on sufficiently long-time behavior and at early stage of the evolution (where they are more consistent), and the consequent effects on correlations. The sensitivity of expectation values to initial conditions other than (10) can also be checked. Finally, it definitively appears of interest also to proceed with multi-mode generalization and to examine dynamics of entanglement. We plan to address these issues in the future.

## A. Parametric oscillator equation with Morse-type frequencies: closed form solutions and their Wronskians

In this Appendix, the derivation of closed form solution to the parametric oscillator equation with frequency (16) with  $V_\infty \neq 0$  will be discussed. We will perform a step-by-step analysis drawing special attention on factors affecting the way in which independent solutions for the equation are permitted. After that we compute their Wronskians, whose role is of central importance as well in explicitly determining solutions to the Ermakov equation via formulae (13)-(14). We will provide the analytical treatment for the derivation of independent solutions when  $D_e, V_\infty < 0$  as the other cases follow by proper algebraic adaptments.

### A.1. Case 1: $D_e, V_\infty < 0$

Let us consider a square parametric frequency defined through an inverse Morse potential with a negative nonvanishing asymptotic value, Equation (16) with  $D_e, V_\infty < 0$ . With a change of variable

$$\xi = 2 d b e^{-\frac{t+t_s}{b}}, \quad (\text{A.1})$$

the homogeneous second order linear differential equation (11) reads

$$\frac{d^2 x(\xi)}{d\xi^2} + \frac{1}{\xi} \frac{dx(\xi)}{d\xi} + \left( \frac{d b}{\xi} - \frac{1}{4} + \frac{v^2 b^2}{\xi^2} \right) x(\xi) = 0 \quad (\text{A.2})$$

where the positive parameters  $v = \sqrt{-V_\infty}$  and  $d = \sqrt{-D_e}$  have been defined for convenience. If we let  $x(\xi)$  to be

$$x(\xi) = e^{-\xi/2} \xi^{b v} z(\xi), \quad (\text{A.3})$$

the differential equation (A.2) becomes, upon dividing by  $e^{-\xi/2} \xi^{b v}$ , the confluent hypergeometric equation

$$\xi \frac{d^2 z(\xi)}{d\xi^2} + (\beta - \xi) \frac{dz(\xi)}{d\xi} - \alpha z(\xi) = 0 \quad (\text{A.4})$$

with parameters  $\alpha = \frac{1}{2} + b(v - d)$  and  $\beta = 1 + 2 b v$ . A solution to the confluent hypergeometric equation is the Kummer's function of the first kind  ${}_1F_1[\alpha; \beta; \xi]$  defined as

$${}_1F_1[\alpha; \beta; \xi] = \sum_{n=0}^{\infty} \frac{(\alpha)_n \xi^n}{(\beta)_n}, \quad (\text{A.5})$$

where  $(\alpha)_n = \alpha(\alpha+1)\dots(\alpha+n-1)$  and  $(\alpha)_0 = 1$ . Note that the Kummer's function  ${}_1F_1[\alpha; -n; \xi]$  is not defined for  $n$  non-negative integer, except for the case  $\alpha = -m$  with  $m$  non-negative integer and  $m < n$ . In these cases, other representations of the solutions to (A.2) should be used (for more details here, see Refs. [65]-[66]).

It is easy to show that  $\xi^{1-\beta} {}_1F_1[1+\alpha-\beta; 2-\beta; \xi]$  is another solution to (A.2). In fact, by letting  $z(\xi)$  be

$$z(\xi) = \xi^{1-\beta} v(\xi), \quad (\text{A.6})$$

upon dividing by  $\xi^{1-\beta}$ , equation (A.2) becomes:  $\xi v(\xi) + (2 - \beta - \xi) \dot{v}(\xi) - (1 + \alpha - \beta) v(\xi) = 0$ . We can use a combination of the above solutions to define the Tricomi confluent hypergeometric function  $U[\alpha; \beta; \xi]$  [65],

$$U[\alpha, \beta, \xi] = \frac{\pi}{\sin(\pi \beta)} \left( \frac{{}_1F_1[\alpha; \beta; \xi]}{\Gamma[\beta] \Gamma[1 + \alpha - \beta]} - \xi^{1-\beta} \frac{{}_1F_1[\alpha + 1 - \beta; 2 - \beta; \xi]}{\Gamma[\alpha] \Gamma[2 - \beta]} \right). \quad (\text{A.7})$$

The advantage of the function  $U[\alpha, \beta, \xi]$  is that, even if it does not exist for  $\beta$  integer, it can be extended analytically for all values of  $\beta$ . For most combinations of real or complex  $\alpha$  and  $\beta$ , the two solutions (A.5) and (A.7) are independent. However, if  $\alpha$  is a non-positive integer, then (A.5) and (A.7) are proportional. This is due to the relation [65, 66],

$$U[-n; \alpha; x] = \frac{(\alpha - 1 + n)!}{(\alpha - 1)!} (-1)^n F[-n; \alpha; x] , \quad (\text{A.8})$$

(with  $n = 0, 1, 2, \dots$ ). In these cases we should use  ${}_1F_1[\alpha; \beta; \xi]$  and  $\xi^{1-\beta} {}_1F_1[1 + \alpha - \beta; 2 - \beta; \xi]$  as independent solutions, when they exist.

In the light of all above considerations, we can finally write the independent solutions to Equation (A.2) as

$$x_1(\xi) = e^{-\xi/2} \xi^{bv} U\left[\frac{1}{2} + b(v-d); 1 + 2bv, \xi\right] , \quad x_2(\xi) = e^{-\xi/2} \xi^{bv} {}_1F_1\left[\frac{1}{2} + b(v-d); 1 + 2bv, \xi\right] , \quad (\text{A.9})$$

that in terms of the time variable  $t$  becomes

$$\begin{aligned} x_1(t) &= e^{-d} b e^{-(t+t_s)/b} e^{-tv} U\left[\frac{1}{2} + b(v-d); 1 + 2bv, 2d b e^{-(t+t_s)/b}\right] , \\ x_2(t) &= e^{-d} b e^{-(t+t_s)/b} e^{-tv} {}_1F_1\left[\frac{1}{2} + b(v-d); 1 + 2bv, 2d b e^{-(t+t_s)/b}\right] , \end{aligned} \quad (\text{A.10})$$

for  $\frac{1}{2} + b(v-d) \neq -m$ , with  $m$  non negative integer, and

$$\tilde{x}_1(\xi) = e^{-\xi/2} \xi^{-bv} {}_1F_1\left[\frac{1}{2} - b(v+d); 1 - 2bv, \xi\right] , \quad \tilde{x}_2(\xi) = e^{-\xi/2} \xi^{bv} {}_1F_1\left[\frac{1}{2} + b(v-d); 1 + 2bv, \xi\right] \quad (\text{A.11})$$

that in terms of the time variable  $t$  becomes

$$\tilde{x}_{1,2}(t) = e^{-d} b e^{-(t+t_s)/b} e^{\pm tv} {}_1F_1\left[\frac{1}{2} \mp b(v \pm d); 1 \mp 2bv, 2d b e^{-(t+t_s)/b}\right] , \quad (\text{A.12})$$

for  $\frac{1}{2} + b(v-d) = -m$ , with  $m$  non negative integer (we have omitted the multiplying factors  $e^{\pm tv} (2d b)^{\mp bv}$  in  $x_{1,2}$  and  $\tilde{x}_{1,2}$  that arise after the change of variable  $\xi \rightarrow t$ ).

The Wronskian of the two solutions (A.9) can be easily computed by resorting to the known forms for expansions pertaining small arguments  $\xi$  of special functions involved. So we can take

$$W(x_1(\xi), x_2(\xi)) = \frac{\cos[\pi b(d-v)] \Gamma(\frac{1}{2} + b(d+v))}{\pi \xi} . \quad (\text{A.13})$$

The Wronskian of solutions (A.10) in the independent variable  $t$ , is related to the Wronskian in the independent variable  $\xi$  by means of the relation  $W(x_1(t), x_2(t)) = -b^{-1} \xi W(x_1(\xi), x_2(\xi))$ , giving explicitly

$$W(x_1(t), x_2(t)) = -\frac{\cos[\pi b(d-v)] \Gamma[\frac{1}{2} + b(d+v)]}{\pi b} . \quad (\text{A.14})$$

Analogously, the Wronskian of the two solutions (A.11) is found in the form  $W(\tilde{x}_1(\xi), \tilde{x}_2(\xi)) = -2bv/\xi$ , and the Wronskian of (A.12) in the variable  $t$ , simply related to  $W(\tilde{x}_1(\xi), \tilde{x}_2(\xi))$  via  $W(\tilde{x}_1(t), \tilde{x}_2(t)) = -b^{-1} \xi W(x_1(\xi), x_2(\xi))$ , explicitly becomes  $W(x_1(t), x_2(t)) = 2v$ .

This completes our derivation of the ingredients for expressing in closed form the solutions to the Ermakov equation with the parametric frequency Equation (16) with  $D_e < 0$  and  $V_\infty < 0$ . Note that when  $D_e < 0$  and  $V_\infty = 0$ , two independent solutions to (11) can only be obtained for  $bd \neq m + \frac{1}{2}$ , with  $m$  non negative integer [65]. Their analytical expression, together with the expression for their Wronskian, is simply given by substituting  $v = 0$  into Eqs. (A.10) and (A.14). In particular, for  $bd = \frac{1}{2} + m$ , ( $m = 0, 1, 2, \dots$ ) all the solutions to the confluent hypergeometric equation (A.4) are proportional to the Laguerre polynomials  $L_m(\xi)$  [65].



## A.2. Cases 2, 3 and 4

**Case 2:**  $D_e < 0$ ,  $V_\infty > 0$ . The treatment of Equation (11) in the present case follows a route similar to that of Case 1 in Subsection A.1, and solutions in the  $\xi$  variable (A.1) will be obtained after performing the replacement  $V_\infty \rightarrow -V_\infty$ , i.e.  $v \rightarrow i v$  into (A.2). Since  $x_1(\xi)$  and  $x_2(\xi)$  are now complex functions, for the evaluation of  $\sigma$  we use the functions  $y_1(\xi) = x_1(\xi) + x_1^*(\xi)$  and  $y_2(\xi) = x_2(\xi) + x_2^*(\xi)$ . In this way the Wronskian becomes, in the original independent variable  $t$ ,

$$W(y_1(t), y_2(t)) = -\frac{2}{\pi b} \left\{ \cos[\pi b(d - i v)] \Gamma \left[ \frac{1}{2} + b(d + i v) \right] + \cos[\pi b(d + i v)] \Gamma \left[ \frac{1}{2} + b(d - i v) \right] \right\}. \quad (\text{A.15})$$

**Case 3:**  $D_e, V_\infty > 0$ . The solution to (11) in the  $\xi$  variable will be obtained with the replacement  $\xi \rightarrow i \xi$ ,  $v \rightarrow i v$  and  $d \rightarrow i d$  into formulae of Subsection A.1, see e.g. Eqs. (A.1)–(A.2). Since  $x_1(\xi)$  and  $x_2(\xi)$  are once again complex functions, for the evaluation of  $\sigma$  we proceed as in Case 2. The final expression that we get for the Wronskian is

$$W(y_1(t), y_2(t)) = -\frac{2}{\pi b} \left\{ \cos[b \pi(d - v)] \Gamma \left[ \frac{1}{2} - i b(d + v) \right] + \cosh[b \pi d] \cosh[b \pi v] \Gamma \left[ \frac{1}{2} + i b(d + v) \right] \right\}. \quad (\text{A.16})$$

**Case 4:**  $D_e > 0$ ,  $V_\infty < 0$ . Replacements  $\xi \rightarrow i \xi$  and  $d \rightarrow i d$  are performed into formulae of Sub. A.1 from (A.1) on.

## References

- [1] V.V. Dodonov and V.I. Man'ko Eds, *Theory of Nonclassical States of Light*, Taylor and Francis, London, 2003.
- [2] A. Nerukh et al., *Non-stationary electromagnetics*, Boca Raton, Pan Stanford Publishing, 2012.
- [3] I.A. Pedrosa, *Quantum electromagnetic waves in nonstationary linear media*, Phys. Rev. **A83**, 032108 (2011).
- [4] D.K. Kalluri, *Electromagnetics of time varying complex media: frequency and polarization transformer*, Boca Raton, CRC Press 2018.
- [5] F. Major, V.N. Gheorghe, G. Werth, *Charged Particle Traps. Physics and Techniques of Charged Particle Field Confinement*, Springer, Berlin, 2005.
- [6] S. Longhi and S.M. Eaton, *Optical realization of the dissipative quantum oscillator*, Opt. Lett. **41**, 1712-1715 (2016).
- [7] D. Hucul et al., *On the transport of atomic ions in linear and multidimensional ion trap arrays*, Quantum Inf. Comput. **8**, 0501-0578 (2008).
- [8] E. Torrontegui et al., *Shortcuts to adiabaticity*, Adv. At. Mol. Opt. Phys. **62**, 117-169 (2013).
- [9] A.D. Sakharov, *The Initial Stage of an Expanding Universe and the Appearance of a Nonuniform Distribution of Matter*, Sov. Phys. JETP **22**, 241-249 (1966). [Russian original: ZhETF, 49, 345 (1965)]
- [10] L.P. Grishchuk and Y.V. Sidorov, *Squeezed quantum states of relic gravitons and primordial density fluctuations*, Phys. Rev. **D42**, 3413 (1990).
- [11] M. Maggiore, *Gravitational wave experiments and early universe cosmology*, Phys. Rep. **331**, 283-367 (2000).
- [12] A. Geralico et al., *A novel approach to the study of quantum effects in the early Universe*, Phys. Rev. **D69**, 043504 (2004).
- [13] G. Landolfi and G. Soliani, *Trans-Planckian effects in nonlinear-dispersion cosmologies*, Phys. Lett. **B588**, 1 (2004).
- [14] D. Brizuela et al., *Quantum-gravity effects for excited states of inflationary perturbations*, Phys. Rev. **D99**, 104007 (2019).
- [15] Ş.A. Büyükaşık and O. K. Pashaev, *Exactly solvable Madelung fluid and complex Burgers equations: a quantum Sturm-Liouville connection*, J. Math. Chem. **50**, 2716-2745 (2012).
- [16] F. Haas and L.G.F. Soares, *Nonlinear oscillations of ultra-cold atomic clouds in a magneto-optical trap*, Physics of Plasmas **25**, 012310 (2018).
- [17] C. Braggio et al., *A novel experimental approach for the detection of the dynamic Casimir effect*, Europhys. Lett. **70**, 754-760 (2005).
- [18] V. Gurarie and J.T. Chalker, *Some generic aspects of bosonic excitations in disordered systems*, Phys. Rev. Lett. **89**, 136801 (2002);
- [19] E.V. Goldstein and P. Meystre, *Quasiparticle instabilities in multicomponent atomic condensates*, Phys. Rev. **A55**, 2935 (1997).
- [20] H. Pu and N. P. Bigelow, *Properties of Two-Species Bose Condensates*, Phys. Rev. Lett. **80**, 1134 (1998).
- [21] V.I. Yukalov, *Difference in Bose-Einstein condensation of conserved and unconserved particles*, Laser Phys. Lett. **1**, 435 (2004).
- [22] S. Robertson, F. Michel, and R. Parentani, *Controlling and observing nonseparability of phonons created in time-dependent 1D atomic Bose condensates*, Phys. Rev. **D95**, 065020 (2017).
- [23] G. I. Martone et al., *Momentum distribution and coherence of a weakly interaction Bose gas after a quench*, Phys. Rev. A **98**, 063617 (2018).
- [24] J. Pietraszewicz, M. Stobinska and P. Deuar, *Correlation evolution in dilute Bose-Einstein condensates after quantum quenches*, Phys. Rev. **A99**, 023620 (2019).
- [25] V. V. Dodonov and A. V. Dodonov, *Quantum harmonic oscillator and nonstationary Casimir effect*, J. Russian Laser Res. **26**, 445-483 (2005).
- [26] C-L. Hung, V. Gurarie and C. Chin, *From Cosmology to Cold Atoms: Observation of Sakharov Oscillations in a Quenched Atomic Superfluid*, Science **341**, 1213-1215 (2013).
- [27] V. Ginis et al., *Frequency converter implementing an optical analogue of the cosmological redshift*, Opt. Express **18**, 5350-5355 (2010).
- [28] P. D. Nation et al., *Colloquium: Stimulating uncertainty: Amplifying the quantum vacuum with superconducting circuits*, Rev. Mod. Phys. **84**, 1-24 (2012).
- [29] R-Y. Zhang et al., *Time circular birefringence in time-dependent magnetoelectric media*, Sci. Rep. **5**, 13673 (2015).
- [30] S-R. Lin et al, *Electromagnetic wave propagation in time-dependent media with antisymmetric magnetoelectric coupling*, Phys. Lett. **A380**, 2582-2587 (2016).
- [31] A. M. Zagorskin et al., *Controlled Generation of Squeezed States of Microwave Radiation in a Superconducting Resonant Circuit*, Phys. Rev. Lett. **101**, 253602 (2008).
- [32] A.M. Zagorskin, E. Il'ichev and F. Nori, *Heat cost of parametric generation of microwave squeezed states*, Phys. Rev. **A85**, 063811 (2012).

- [33] Ş.A. Büyükaşık and Z. Çayıç, *Time-evolution of squeezed coherent states of a generalized quantum parametric oscillator*, J. Math. Phys. **60**, 062104 (2019).
- [34] R.G. Littlejohn, *The semiclassical evolution of wave packets*, Phys. Rep., **138**, 193-291 (1986).
- [35] M. Andrews, *Invariant operators for quadratic hamiltonians*, Am. J. Phys. **67**, 336 (1999).
- [36] D. Schuch, *Quantum Theory from a Nonlinear Perspective. Riccati Equations in Fundamental Physics*, Fundamental Theories of Physics **191**, Springer, Berlin, 2018.
- [37] V.V. Dodonov and V.I. Man'ko, *Invariants and the Evolution of Nonstationary Quantum Systems*, in: Proceedings of Lebedev Physics Institute, Acad. Sci. U. S. S. R., Vol. 183, Nova Science Publishers, Commack N. Y., 1989.
- [38] V. N. Chernega and O.V. Man-ko, *Coherent states of parametric oscillators in the probability representation of quantum mechanics*, J. Russian Laser Research, **41**, 11-22 (2020).
- [39] H.P. Robertson, *The uncertainty principle*, Phys. Rev. **34**, 163-164 (1929).
- [40] F.J. Narcowich, *Geometry and uncertainty*, Journal of Mathematical Physics, **31**, 354-364 (1990).
- [41] M. de Gosson, *Uncertainty Principle, Phase Space Ellipsoids and Weyl Calculus*, in: *Operator Theory: Advances and Applications*, Vol. 164, Birkhäuser Verlag, Basel/Switzerland 2006; pp. 121-132.
- [42] Ya. Eliashberg, S. Kim and L. Polterovich, *Geometry of contact transformations and domains: Orderability versus squeezing*, Geom. Topol. **10**, 1635-1747 (2006).
- [43] G. Profilo and G. Soliani, *Group-theoretical approach to the classical and quantum oscillator with time-dependent mass and frequency*, Phys. Rev. **A44** 2057 (1991).
- [44] H.R. Lewis and W. B. Reisenfeld, *An Exact Quantum Theory of the Time-Dependent Harmonic Oscillator and of a Charged Particle in a Time-Dependent Electromagnetic Field*, J. Math. Phys. **10**, 8 (1969).
- [45] A. Mostafazadeh, *Time-Dependent Diffeomorphisms as Quantum Canonical Transformations and the Time-Dependent Oscillator*, J. Phys. A: Math. Gen. **31**, 6495-6503 (1998).
- [46] D. F. Walls and G.J. Milburn, *Quantum Optics*, Springer Verlag, Berlin, 2008.
- [47] G. Landolfi, G. Ruggeri, and G. Soliani, *A note on the loss of coherence in wave packets squeezed systems*, Int. J. Quant. Inform. **2**, 529-540 (2004).
- [48] M. Gianfreda and G. Landolfi, *Wave packets and statistics concerned with SUSY-QM partners of Paul-trap hamiltonians*, Theor. Math. Phys. **168**, 924-938 (2011).
- [49] O. Došlý, *On some aspects of the Bohl transformation for Hamiltonian and symplectic systems*, J. Math. Anal. Appl. **448**, 281-292 (2017).
- [50] C. Athorne, *Stability and periodicity in coupled Pinney equations*, J. Diff. Eq. **100**, 82 (1992).
- [51] C. Rogers, *On a canonical nine-body problem. Integrable Ermakov decomposition via reciprocal transformations*, J. Nonlin. Math. Phys. **26**, 98-106 (2019).
- [52] C. Rogers and W.K. Schief, *Ermakov-type systems in nonlinear physics and continuum mechanics*, in *Nonlinear Systems and Their Remarkable Mathematical Structures*, N. Euler (ed.), CRC Press, Boca Raton Fl, 2018.
- [53] P. G. L. Leach and K. Andriopoulos, *Ermakov equation: a commentary*, Appl. Anal. Discrete Math. **2**, 146-157 (2008), and Refs. therein.
- [54] A. Matzkin, *Smooth amplitude-phase formulation of the Schrödinger equation based on the Ermakov invariant*, Phys. Rev **A63** 012103 (2000).
- [55] K-E Thylwe, *The barrier transmission problem treated by the amplitude-phase method and expressed in terms of an invariant of the Ermakov-Lewis type*, J. Phys. A: Math. Gen. **38**, 235-243 (2005).
- [56] R. Auzzi et al., *Time-dependent stabilization in AdS/CFT*, JHEP 2012, 35 (2012).
- [57] V. P. Ermakov, *Transformation of differential equations*, Univ. Izv. Kiev **20**, 1-19 (1880); transl. : Appl. Anal. Discrete Math. **2**, 123 (2008).
- [58] P. Bohl, *Über eine Differentialgleichung der Störungstheorie*, J. Reine Angew. Math. **131**, 268-321 (1906).
- [59] S. Goff and D.F. St. Mary, *The transformation for second order linear differential systems*, J. Math. Anal. Appl. **140**, 95-106 (1989).
- [60] For a recollection of main results achieved in the various cases of interest, see e.g.: Q Kong and M. Pašić, *Second-order differential equations: some significant results due to James S.W. Wong*, Differ. Equ. App. **6**, 99-163 (2014).
- [61] A. Zettl, *Sturm-Liouville theory*, Mathematical surveys and monographs, 121, AMS, Providence, 2005.
- [62] R. Bellman, *Perturbation techniques in mathematics, physics, and engineering*, Holt, Rinehart and Winston Inc., New York, p. 85, 1966.
- [63] H. Cruz et al. *Time-evolution of quantum systems via a complex nonlinear Riccati equation. I. Conservative systems with time-independent Hamiltonian*, Ann. Phys. **360**, 44-60 (2015).
- [64] C. M. Bender and S. A. Orszag, *Advanced Mathematical Methods for Scientists and Engineers*, Springer-Verlag, New York, 1999.
- [65] Abramowitz, M. and Stegun, I. A. (Eds.). *Handbook of Mathematical Functions with Formulas, Graphs, and Mathematical Tables*, New York: Dover, p. 504-505, 1972;
- [66] D. Zwillinger, *Handbook of Differential Equations*, 3rd ed. Boston, MA: Academic Press, p. 123, 1997.